F. Suárez, L. Felipe-Sesé, F.A. Díaz, J.C. Gálvez, M.G. Alberti, On the fracture behaviour of fibre-reinforced gypsum using micro and macro polymer fibres, Construction and Building Materials, Volume 244, 2020, 118347, ISSN 0950-0618, https://doi.org/10.1016/j.conbuildmat.2020.118347 .

On the fracture behaviour of fibre-reinforced gypsum using micro and macro polymer fibres

F. Suárez[a], L. Felipe-Sesé[a], F.A. Díaz[b], J.C. Gálvez[c], M.G. Alberti[c]

[a] *Departamento de Ingeniería Mecánica y Minera. Universidad de Jaén. Campus Científico-Tecnológico de Linares. Cinturón Sur 23700 – Linares (Jaén), Spain*
[b] *Departamento de Ingeniería Mecánica y Minera. Universidad de Jaén. Campus Las Lagunillas. 23071 – Jaén, Spain*
[c] *Departamento de Ingeniería Civil-Construcción. Universidad Politécnica de Madrid . E.T.S.I. Caminos, Canales y Puertos, C/ Profesor Aranguren s/n 28040 – Madrid, Spain*

Abstract

Gypsum is the most widely used material as interior lining in buildings due to its low cost and good habitability conditions. The use of fibres as randomly distributed reinforcement of quasibrittle matrices, such as gypsum, remarkably improve the material behaviour under tensile stresses. In this work, the fracture behaviour of gypsum specimens reinforced with several types of polymer fibres was assessed, for one of them three fibre lengths were studied. Three types of polymer fibres were employed, with one of them being of microscopic scale and the other two of macroscopic scale. The mechanical behaviour of each mix was studied by means of three-point bending tests and compression tests that were analysed using a digital image correlation system. To study the influence of the fibre length, pull-out tests were also performed. The size, surface finishing and length of the fibres strongly affect the material properties and the way that the fracture mechanisms are developed.

Keywords: Fibre-reinforced gypsum, Polyolefin fibres, Fracture.

1. Introduction

Due to its low cost as well as good habitability and comfort conditions, gypsum is the most extended material as interior lining in buildings. In the last decades, this industry has developed new solutions, such as sandwich panels of laminated gypsum or the use of cellulose as reinforcement. On another note, the addition of polymer fibres as reinforcement of quasi-fragile matrices greatly improves the behaviour of the base material, making them suitable for new uses. This reinforcement improves the ductility of the material and increases the fracture energy that the material can absorb before completely losing their load-bearing capacity. This aspect is of particular interest in elements that can experience impact loading or seismic effects, and it has been adopted and studied in the last years in the field of concrete [1, 2, 3, 4]. The Model Code for Concrete Structures [5], as well as other structural concrete standards [6, 7, 8], already include guidelines for the use of fibres as structural reinforcement in concrete. Nevertheless, although this normative seems to reproduce well elements reinforced with steel fibres, there is not enough confidence when other types of fibres are adopted [9].

There are studies about the mechanical properties of fibre reinforced gypsum (FRG) as those by García-Santos [10, 11], which studied the mechanical properties of gypsum reinforced with several types of polymer fibres. Nowadays, the study of how different additions affect the properties of gypsum is still of interest, since in some cases the thermal properties can be enhanced [12] and in other cases the mechanical properties improved [13, 14]. The use of natural fibres, such as hemp or flax, is also appealing, since they can improve the mechanical, acoustic and thermal properties of gypsum in an eco-friendly manner [15, 16, 17]. In any case, the addition of fibres in matrices with low strength under tension, such as concrete or gypsum, usually induces

*F. Suárez
Email address: fsuarez@ujaen.es (F. Suárez)

a better mechanical behaviour that can extend their use to other areas. This has been recently observed with polyolefin fibre reinforced concrete (PFRC), which has already been used as the only reinforcement in structural concrete [18, 19, 20, 21].

When the mechanical properties of FRG have been studied, the mechanical tests were usually reduced to obtaining the compression strength, the elastic modulus and the flexural strength [10, 22, 23]. However, the fracture energy absorbed by the material before completely losing its load-bearing capacity is of significant importance in some cases. It is a key enhancement of FRG when compared with plain gypsum. This material property should also be taken into account for characterising the performance of the material.

In this work, the mechanical properties of FRG specimens, made with several types of polymer fibres, were studied. Three types of polymer fibres were considered, with one of them being micro and the other two macro. Each of these fibres were mixed with gypsum using two proportions, 5 and 10 kg/m^3, and in the case of one of the macrofibres, three lengths were used: 24, 48 and 60 mm. The study was performed by testing specimens under compression and under a three-point bending test on notched specimens, which also provides information about the fracture energy released by the material before the specimen collapses. Finally, in the case of one of the macrofibres, pull-out tests were performed in order to explain some remarkable differences observed in the flexural behaviour of specimens made with this type of fibres but using different fibre lengths. As discussed below, the pull-out test is only carried out with one type of the macro-fibres used in this study, given that for reasons that will be explained later, the use of this test with the other fibres make the results hard to analyse.

The use of a digital image correlation system (DIC) has provided interesting information about how the fibres modify the fracture mechanisms of quasibrittle materials [24, 25]. In this study, it allowed keeping track of certain parameters in the three-point bending test and obtaining the complete strain field on the specimens surface, which helped to identify how the use of different types of fibres modified the fracture behaviour of the material.

2. Design of the study

The main aim of this study was to analyse the behaviour of FRG when polymer fibres of different size scales were employed. To do this, three types of fibres were selected, one of them being of microscopic size and two of them being macroscopic, identifying the microscopic fibres with letter A and the two macroscopic fibres with letters B and C, as shown in Figure 1. In the case of the microscopic fibre, it resembles short textile fibres gathered in small bundles. Both macroscopic fibres are made of the same polymer but have different shapes and surface finishing. In the case of fibre B, the fibre surface is mainly smooth and the endings show ramifications, while the surface of C fibres is embossed and no ramifications can be observed at the endings

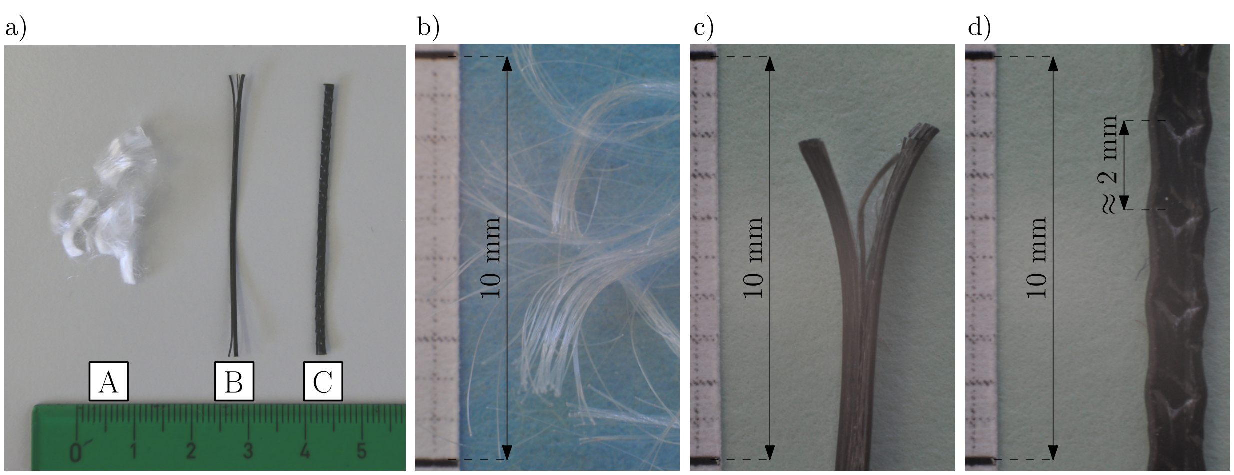

Figure 1: Fibres used in this study: a) General view and nomenclature, b) detail of A type fibres, c) detail of ending in B type fibres and d) detail of the embossed surface of C type fibres.

This study analysed the following aspects regarding polymer fibre reinforcement of gypsum:

Table 1: Gypsum mix proportions (fibre proportions expressed in kg/m^3)

Mix	w/g	A fibres	B fibres	C fibres		
				L=24 mm	L=48 mm	L=60 mm
0	0.63	–	–	–	–	–
A5	0.63	5	–	–	–	–
A10	0.63	10	–	–	–	–
B5	0.63	–	5	–	–	–
B10	0.63	–	10	–	–	–
C5-L24	0.63	–	–	5	–	–
C10-L24	0.63	–	–	10	–	–
C5-L48	0.63	–	–	–	5	–
C10-L48	0.63	–	–	–	10	–
C5-L60	0.63	–	–	–	–	5
C10-L60	0.63	–	–	–	–	10

- Difference on the mechanical properties of FRG mixes made using micro and macro polymer fibres.
- Difference on the behaviour of FRG mixes using macro fibres with different surface finishing.
- Influence on the fibre proportion on the mechanical properties for each of the fibres considered in the study.
- Influence of the fibre length when using polymer macro-fibres.

Therefore, 11 sets of three specimens each were prepared, one of plain gypsum with no fibres added, which will serve as reference (0), two with microscopic A fibres employing fibre dosages of 5 and 10 kg/m^3 (A5 and A10), two with macroscopic B fibres employing the same fibre dosages mentioned (B5 and B10) and six with macroscopic C fibres combining the two mentioned fibre dosages and three fibre lengths of 24, 48 and 60 mm (C5-L24, C5-L48, C5-L60, C10-L24, C10-L48 and C10-L60). Regarding the amount of water added in each mix, the water to gypsum ratio (w/g) was obtained following the procedure described in the standard [26], which determines the mass of gypsum that can be saturated when it is sprinkled into 100 g of water. Table 1 summarises this information.

3. Experimental work

This section presents the materials used for manufacturing the various sets of specimens described above and the experimental tests carried out, including a description of the experimental setups and tools used.

3.1. Materials and mixes

Gypsum

Selected gypsum corresponds to plaster, classified as A1 according to the EN 13279-1 standard [27], composed by hemihydrated calcium sulphate ($CaSO_4 \cdot 0.5\ H_2O$). This material is commonly used for manufacturing precast elements such as plasterboard panels used in sandwich-type partitions.

Fibres

Three types of fibres were used in this study, they can be seen in Figure 1. Fibres A are polypropylene microfibres, named Sikafiber M-12, that are usually employed in concrete and mortars for reducing their cracking and increasing their durability. They are 12 mm long and have a diameter of 31 μm. Fibres B are polyolefin macrofibres with a length of 48 mm, equivalent diameter of 0.92 mm and smooth finishing surface, presenting ramifications at their endings. Finally, C-type fibres are also polyolefin macrofibres, but their aspect is different from B-type fibres, they are thicker and their surface is embossed with a pattern that repeats every 2 mm along them (a more detailed description can be found in [4]). Regarding C-type fibres, three lengths are used: 24, 48 and 60 mm.

3.2. Specimens

Sets of three 160×40×40 mm^3 prismatic specimens of each gypsum mix were manufactured following a slight variation of the procedure described in UNE-EN 13279-2 [26] for adding the fibres. Such procedure is described below:

1. Gypsum was poured on the water and manually mixed for 40 seconds.
2. Fibres were added and mixed manually for 20 seconds.
3. Mixing continued for 60 more seconds in a planetary mixer at low speed.
4. Moulds, previously impregnated with release agent, were filled.
5. Moulds were hit to eliminate air bubbles and finally levelled.
6. The specimens were unmoulded and cured inside a controlled-climate chamber for seven days at 23±2^{o}C and relative humidity of 50±5%.
7. Specimens were dried inside an oven at 50^{o}C for 48 hours.
8. Specimens were cooled at room temperature and the notch was cut with a band saw by dry way.
9. Specimens were marked with black spray for the later use of digital image correlation (DIC).

3.3. Digital image correlation (DIC)

A digital image correlation system was used to measure strains in the three-point bending tests and the compression tests. This technique is based on comparing images of a specimen obtained during a test with the initial unloaded image of the specimen; this comparison allows obtaining the displacement field on a desired region of the specimen, thus, the derived strain field can be easily obtained. For more information on this technique, the reader can consult [28, 29]. In this work an Allied Stingray F-080C with a resolution of 1032×766 pixels was used and the software Vic-2D, by Correlated Solutions, was employed [30]. Digital image correlation in 2D was performed by employing a 21 pixels size facet and 5 pixels of step.

3.4. Experimental setup of the three-point bending test

Figure 3a shows a scheme of this test. In this study the span length was $L = 100$ mm, the specimen height $h = 40$ mm and the notch length $a = 13$ mm. Therefore, a span/height relation of 2.5 and a notch of 1/3 the height of the specimen have been considered. The tests were carried out with a dual column testing system of Instron of the 5960 series and using a load cell of 30 kN of capacity. For these tests, the specimens were placed over two cylindrical rolls supported by a horizontal beam and the load was vertically applied, as shown in Figure 3b. The load was applied at low speed (0.05 mm/min) up to the first load decay, in order to reduce the dynamic effect of such a load drop to a minimum, and 0.25 mm/min later. The duration of the test was of 27 minutes for each specimen and images for DIC were capture every 5 seconds.

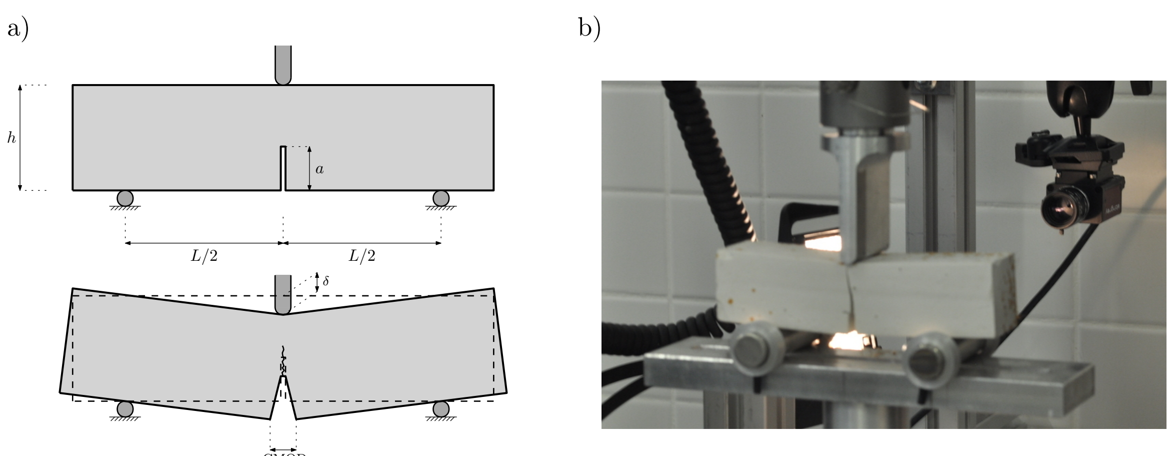

Figure 2: Experimental setup of the three-point bending test on a notched specimen: a) specimen dimensions and displacement parameters; b) experimental setup arranged for the use of DIC.

3.5. Experimental setup of the compression test

After the three-point bending test was carried out, the specimens were cut using a band saw by dry way, obtaining two 40 mm side cubic samples out of each prismatic specimen. These tests were performed following the UNE-EN 13279-2 standard [26], placing each specimen between two cylindrical plates and using the same testing equipment described for the three-point bending tests. The load was applied at a speed of 1 mm/min up to a total displacement of 3 mm and the images for DIC were captured every second.

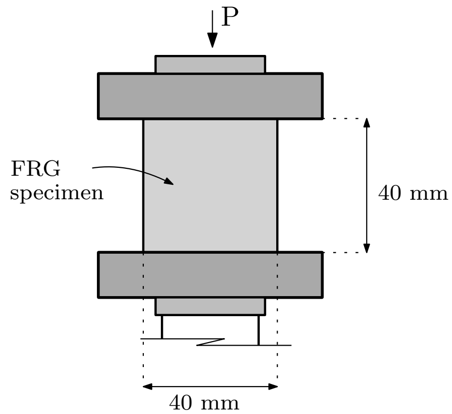

Figure 3: Experimental setup and dimensions of the compression test.

3.6. Experimental setup of the pull-out test

The pull-out allows assessing the quality of the bonding mechanism between the fibres and the matrix in a composite material. In this study, the specimens were manufactured by embedding a fibre up to a certain length inside fresh gypsum, then the standard process of curing and drying described before was applied.

The test consists of pulling a fibre out of the gypsum matrix to obtain a load-slip diagram that identifies the load bearing capacity of the fibre-matrix bonding and how it evolves as the fibre is progressively extracted from the matrix. Figure 4 shows a scheme of the test (a) and images of one of the test at different stages (b). Apart from the displacement due to the fibre being pulled out of the gypsum matrix, the displacement of the grip may cause slipping between the clamping jaws and the fibre, which would make the displacement measure invalid or not correct. To detect this possible problem and easily identify the tests that must be discarded, four tracking points were attached, one on the clamping jaws, one on the top region of the fibre, one on the bottom part of the fibre and, finally, another one on the gypsum block. The first two allow identifying a possible slipping between the jaws and the fibre and the last two allow measuring the true pull-out displacement during the test. To measure the displacement of each of these points, the ImageJ software [31] was used, which allows precise and easy tracking of the target points. This test was carried out with a load displacement of 1.2 mm/min and capturing one image per second.

4. Results and discussion

This section presents the experimental results. In order to make them easier to read, the results corresponding to plain gypsum (O) are shown in black, those corresponding to polypropylene microfibres (A) are shown in red, those of type B macrofibres are shown in green and those of type C macrofibres are shown in blue. Different fibre dosages and different fibre lengths in the case of B fibres are conveniently identified and marked in each graph.

4.1. Fresh state workability

Although no specific test was carried out to measure the workability of the mixes, significant differences were found in this aspect when using micro or macrofibres. When macrofibres B or C were employed, the workability of the mix in fresh state was good with the fibre proportions analysed (5 and 10 kg/m^3). When microfibres A were used, the mix became much thicker, which was particularly noticeable with the higher

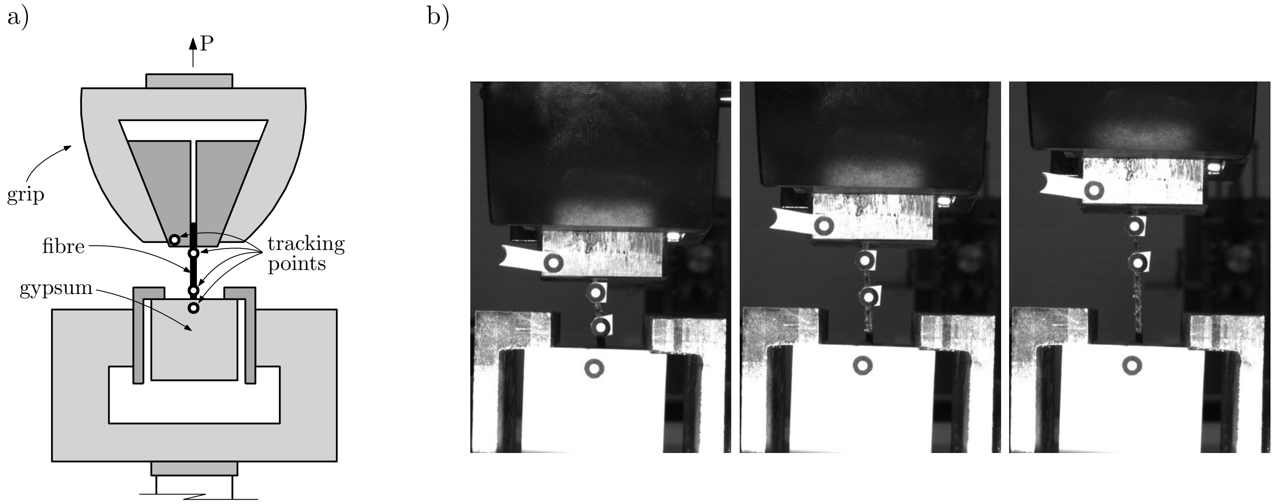

Figure 4: Experimental setup of the pull-out test a) scheme of the setup and b) images of a pull-out test at different instants.

fibre proportion. This was expected, since the microscopic nature of this fibre leads to a higher specific surface area, thus leading to a higher amount of water attached to them. Nevertheless, this suggests that in the case of B or C fibres, higher fibre proportions could be added, but in the case of A fibres, the amount of fibres that can be added is clearly limited by the workability of the mix.

4.2. Three-point bending test

Figures 5, 6 and 7 show the diagrams experimentally obtained for specimens with A, B and C fibres, respectively, using three specimens with each mix. On the left of each figure, the load-displacement diagram is shown and, on the right, the load-CMOD diagram is presented, with CMOD being the crack mouth opening displacement obtained with DIC. In all cases, the results obtained for each fibre dosage, 5 and 10 kg/m^3, are presented together, showing the experimental envelope for each as a shade and the average results (of three specimens) of each dosage with different line styles (dashed for 5 kg/m^3 and continuous for 10 kg/m^3). The average result of plain gypsum (O) is also included in the load-displacement diagrams as a continuous black line, although it is barely visible given that it only develops in the very first instants of the test; as for the load-CMOD diagrams, it is not included, since it would not be visible at all.

Looking at Figure 5, it can be observed that polypropilene microfibres extend the flexural behaviour of gypsum, which becomes remarkably ductile. Unlike plain gypsum, those specimens reinforced with fibre A showed a load recovery after the first load peak, extending the specimen flexural strength beyond 5 mm of load displacement. The first load peak identifies the moment at which the gypsum matrix failed and the fibres became the main mechanism of resistance. The energy released by this fracture process is much higher than in the case of plain gypsum, that shows an almost negligible absorbed energy before losing its load-bearing capacity. When 5 kg/m^3 were added, the enhancement is clearly observed and when 10 kg/m^3 were added, the post-peak strength becomes approximately twice as higher. It is worth noting that the diagrams are smooth, not showing abrupt load changes during the fracture processes.

As regards those specimens manufactured with B macrofibres, Figure 6 shows an analogous behaviour as that observed for specimens manufactured with A microfibres. There was also an important load recovery after the first peak that gradually reached a new maximum and slowly lost its load-bearing capacity. Those specimens with 10 kg/m^3 also showed a higher load-bearing capacity after the first peak compared with those with 5 kg/m^3, although not being as much as twice their maximum recovery load. It is interesting to observe two main differences with regard to the specimens made with A fibres: the load-bearing capacity after the first peak is remarkably high, even leading to a maximum load recovery higher than the first peak, and the experimental repetitiveness in the case of B fibres was significantly lower.

Figure 7 shows the diagrams for all the specimens manufactured with C macrofibres, that is to say, a total of 18 specimens, three per mix. One of the main differences that can be observed concerns the remarkable improvement in the flexural behaviour that was obtained just by modifying the fibre length. When fibres were 24 mm long, the specimens showed a very limited load recovery after the first peak if their behaviour is compared with those obtained with 48 and 60 mm long fibres. The same proportion of fibres with shorter length of these implied a higher number of fibres in the fracture surface of the specimen, which increased the probability of finding more fibres in the crack path, thus a better behaviour could be expected, nevertheless, the experimental results showed a poorer performance when 24 mm fibres were used. It is also interesting to observe that if the results with 48 and 60 mm long fibres are compared, the behaviour is quite similar, even reaching slightly higher recovery loads after peak-load with the latter. Using longer fibres imply fewer fibres in the specimen, therefore, a lower number of fibres crossing the crack path is expected; nevertheless, the experimental results show that it can be beneficial to use longer fibres, even if that reduces the number of them in the mix. Regarding the overall aspect of the diagrams, and not taking into account those of 24 mm long fibres, which are not able to show the load-bearing capacity of this type of fibres, it is interesting to observe that the experimental scatter was very high and that the diagrams showed very often abrupt load changes, which is related to fibres losing their grip with gypsum, thus leading to discrete load drops. It is also worth noting that the longer the fibre, the maximum load after the first peak was observed, taking place at around $\delta = 0.5$ mm in the case of 24 mm long fibres, at around $\delta = 1.75$ mm with 48 long fibres and at around $\delta = 2$ mm with 60 mm long fibres. This agrees with the observations made for polyolefin fibre reinfoced concrete in [32] and [33]. It should be mentioned that the better orientation factor expected for the longer fibres given the relation fibre length/specimen size explains this enhancements proportional with the fibre length and could be considered as expected.

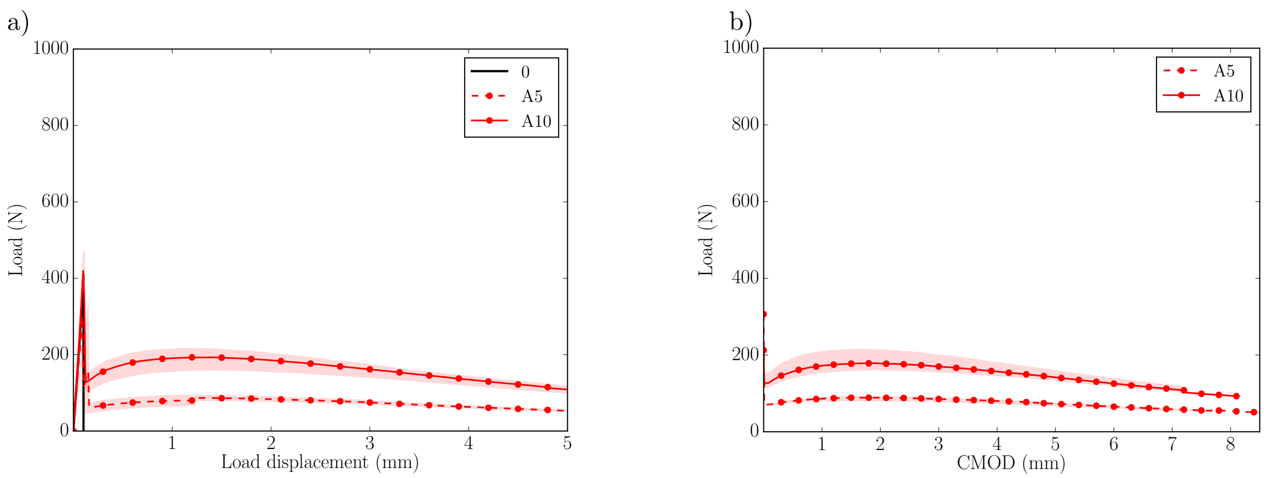

Figure 5: Experimental results of the three-point bending tests on specimens manufactured with A fibres (shaded areas represent the experimental envelopes).

In order to measure the energy released by each mix and compare their performance, this value has been measured for each at three instants of the test corresponding to load displacements of 1, 3 and 5 mm. These values of the specific fracture energy are obtained by computing the area below the curves in the load-load displacement diagrams presented before up to the corresponding value of the considered load displacement and dividing it by the area of the fracture surface, which in this case is a 27 mm×40 mm rectangle. Table 2 lists these values, which are graphically shown in Figure 8. Regarding the reference mix of plain gypsum, O, the value is equal for all the values of δ, since once the maximum load peak is reached, no additional energy is absorbed by the specimen. Regarding those specimens manufactured with any type of fibres, the specific fracture energy increases with δ, although significant differences may be remarked. In the case of the specimens made with the microfibres (A5 and A10) and the specimens made with short C macrofibres (C5-L24 and C10-L24), the energy increase is quite limited; in the case of the former it seems that this performance could be enhanced by increasing the fibre dosage, since the energy is about twice in the case of A10 with respect to A5. Conversely, in the case of the specimens made with 24 mm long C fibres, the fibre dosage does not seem to boost this value.

As for the rest of the fibres, B macrofibres and 48 and 60 mm long C macrofibres, the specific fracture energy is very significant, even leading to high values of more than 100 times those of plain gypsum when

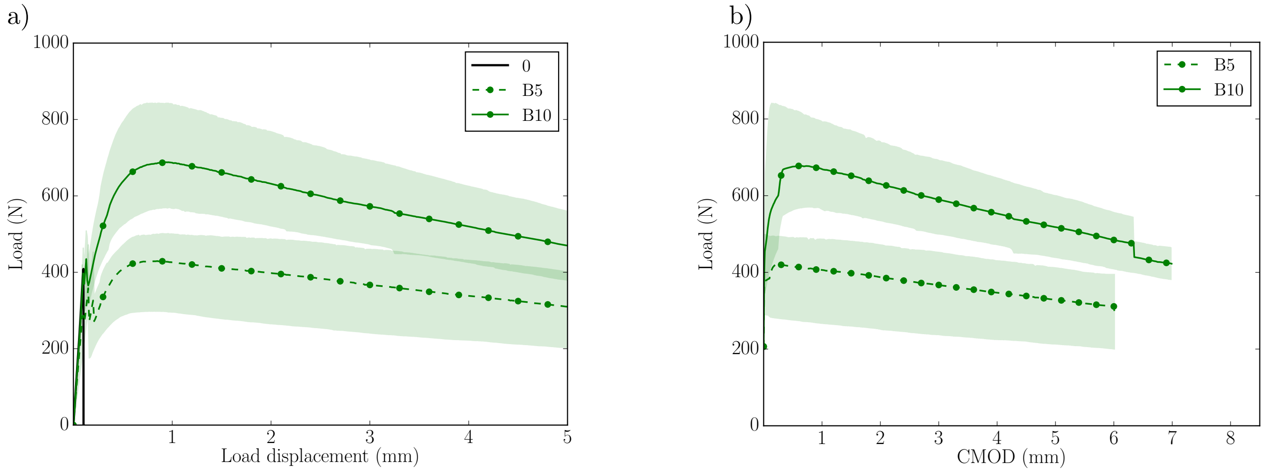

Figure 6: Experimental results of the three-point bending tests on specimens manufactured with B fibres (shaded areas represent the experimental envelopes).

Table 2: Specific fracture energy in N/m at different load displacements and ratio with respect to mix 0.

Mix	Load displacement					
	1 mm		3 mm		5 mm	
	G_F (N/m)	$\frac{G_{Fi}}{G_{F0}}$	G_F (N/m)	$\frac{G_{Fi}}{G_{F0}}$	G_F (N/m)	$\frac{G_{Fi}}{G_{F0}}$
0	23.97	1.00	23.97	1.00	23.97	1.00
A5	77.93	3.25	229.61	9.58	347.01	14.48
A10	164.37	6.86	501.94	20.94	751.86	31.36
B5	337.34	14.07	1072.95	44.76	1699.65	70.90
B10	519.72	21.68	1687.27	70.38	2649.93	110.54
C5-L24	96.09	4.01	181.29	7.56	229.00	9.55
C10-L24	354.71	14.80	1261.63	52.63	1992.61	83.12
C5-L48	392.96	16.39	1448.90	60.44	2322.01	96.86
C10-L48	112.06	4.67	217.73	9.08	263.04	10.97
C5-L60	531.69	22.18	1733.76	72.32	2408.07	100.45
C10-L60	561.69	23.43	2070.04	86.35	3249.15	135.54

$\delta = 5$ mm, which is expected to grow higher at larger values of δ.

Finally, in order to analyse how each type of fibre induced different fracture mechanisms, the value of the CMOD and the load displacement have been compared at an advanced state of the test, specifically at $\delta = 5$ mm. These results can be consulted in Table 3 and are displayed in Figure 9. It can be observed that the use of A type microfibres lead to higher values of the CMOD/δ ratio, especially if the values obtained with 24 long C type fibres are ignored since, as explained before, they are not representative of the possibilities of these fibres as reinforcement of gypsum. A type specimens provide ratios of around 1.4-1.6 while the other specimens give values of 0.9-1.3. This means that the use of A type microfibres tends to produce more visible cracks than the use of B or C types macrofibres. This can be more clearly understood with the help of the DIC results. Figure 10 shows the horizontal strain fields of three specimens obtained with the DIC analysis, which correspond to A5, B5 and C5-L48 specimens. All the three images show the horizontal strain field at the same load displacement ($\delta = 5$ mm), which allows comparing the three types of fibres considered in this study. In the case of the A5 and B5 specimens, damage develops in a very concentrated crack path, following an almost straight line connecting the initial crack tip and the load application point, while in the case of the C5-L48 specimen, the strain field allows identifying several cracks that extend along a certain width of the specimen. Therefore, A type microfibres induce a fracture mechanism that concentrates damage in a single crack while C type macrofibres extend the damage mechanism to a wider region of the specimen, inducing

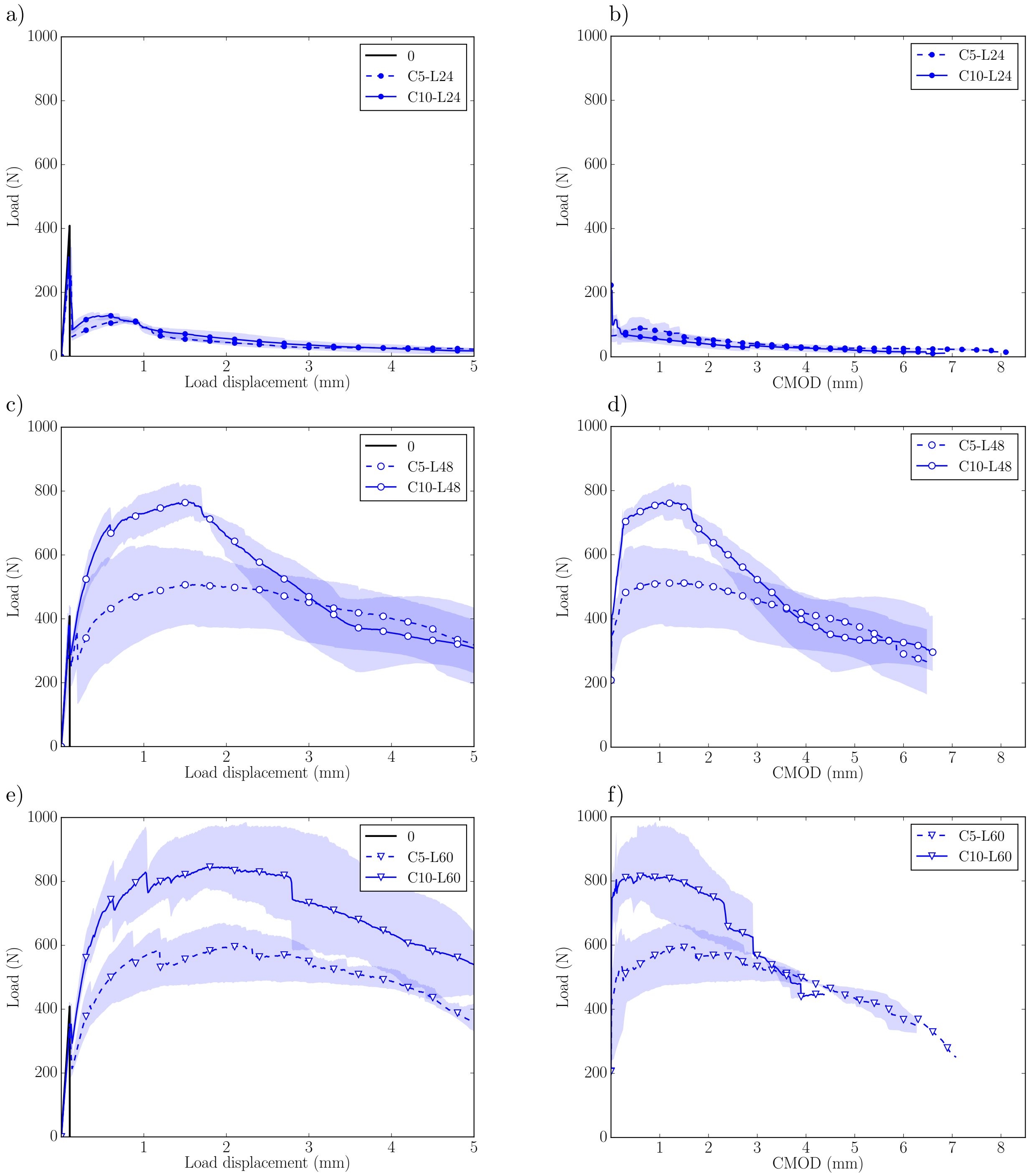

Figure 7: Experimental results of the three-point bending tests on specimens manufactured with C fibres (shaded areas represent the experimental envelopes).

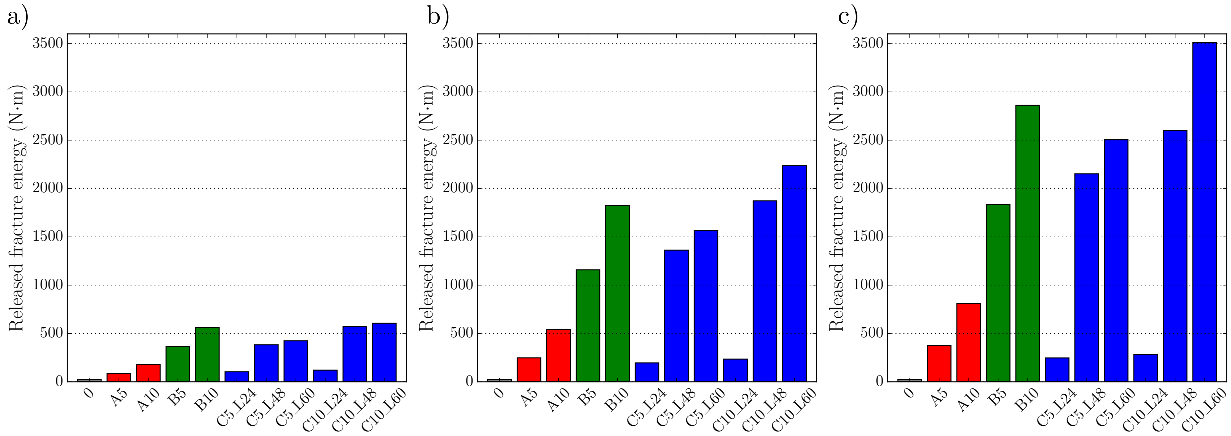

Figure 8: Released energy of each mix at three instants of the test: a) $\delta = 1$ mm, b) $\delta = 3$ mm and c) $\delta = 5$ mm.

Table 3: Comparison of CMOD versus load displacement at $\delta = 5$ mm.

Mix	Load displacement (mm)	CMOD (mm)	CMOD/δ
A5	5.0	8.15	1.63
A10	5.0	7.15	1.43
B5	5.0	5.90	1.18
B10	5.0	6.35	1.27
C5-L24	5.0	7.37	1.47
C10-L24	5.0	5.62	1.12
C5-L48	5.0	5.86	1.17
C10-L48	5.0	6.46	1.29
C5-L60	5.0	6.10	1.22
C10-L60	5.0	4.63	0.93

several small cracks that, as a result, produce a thinner main crack. This results in different values of the crack tip opening displacement, which as the figure clearly shows, is much smaller in the case of C5-L48 specimen when compared with any of the other two specimens.

4.3. Compression test

Figure 11 shows the results obtained with the compression tests for each FRG mix compared with plain gypsum. The values of σ_{max} have been obtained as F_{max}/S with F_{max} being the maximum compression load and S the compression surface ($40{\times}40$ mm^2).

Figures 11c and 11d show that the specimens made with B type fibres and 48 and 60 mm long C type fibres show no significant differences with respect to plain gypsum specimens, only a slight trend to lower values of the maximum compression strength can be highlighted.

The load-displacement diagrams show that the specimens made with A type microfibres tend to have a lower modulus of elasticity and a lower maximum compressive strength, which can also be observed in Figures 11a and 11b, where A5 and A10 show lower peak loads and elastic slopes. This suggests that the microfibres modify the overall elastic mechanical properties of gypsum, giving rise to some extent to a new material with different characteristics. In the case of specimens made of B and C type fibres, these differences are not so evident and it seems that the elastic behaviour of the material is similar to that of plain gypsum.

Figures 11a and 11b also show interesting differences among these mixes. With regard to A type specimens, although the peak load is lower, the load decay after it is smoother, only experiencing a small decrease as the test proceeds. In the case of C type specimens, the pre-peak behaviour is very similar, but after the peak, they show a faster load decrease than A type specimens, while B type specimens show an intermediate load decrease, not as fast as C type ones neither as slow as A type specimens. This suggest that in the case of the

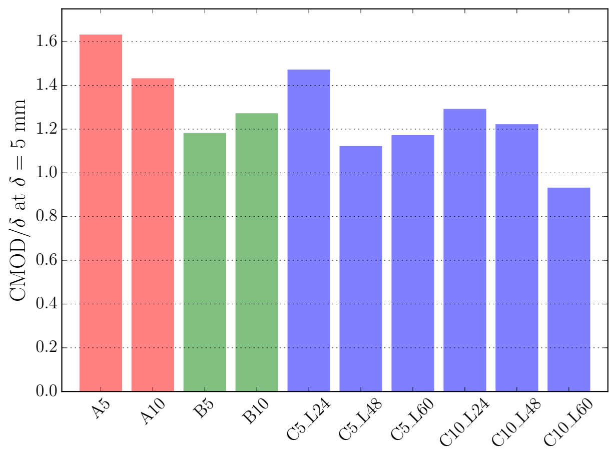

Figure 9: Comparison of the CMOD/δ ratio when $\delta = 5$ mm.

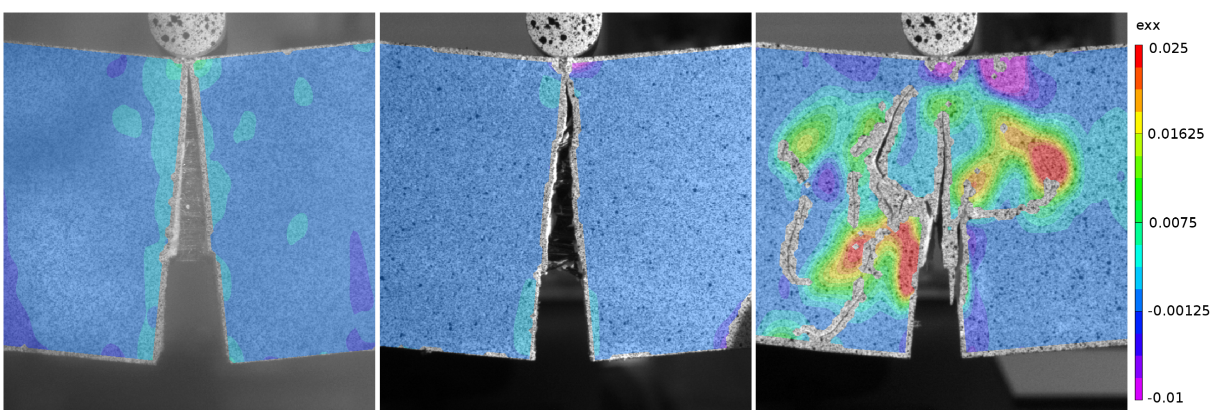

Figure 10: Comparison of ε_x strain fields of A5 (left), B5 (center) and C5-L48 (right) specimens at a load displacement of $\delta = 5$ mm.

Table 4: Values of E and σ_{max} in the compression tests and the corresponding ratios with respect to mix 0; coefficients of variation (or relative standard deviations) are reported in brackets.

Mix	E (MPa)	$\frac{E_i}{E_0}$	σ_{max} (MPa)	$\frac{\sigma_{max_i}}{\sigma_{max_0}}$
0	922.26 (0.03)	1.00	11.94 (0.04)	1.00
A5	797.44 (0.01)	0.86	10.77 (0.11)	0.90
A10	860.59 (0.10)	0.93	9.47 (0.04)	0.79
B5	938.68 (0.06)	1.02	11.73 (0.05)	0.98
B10	897.48 (0.05)	0.97	11.31 (0.10)	0.95
C5-L24	927.86 (0.07)	1.01	12.70 (0.06)	1.06
C5-L48	919.99 (0.08)	1.00	12.16 (0.07)	1.02
C5-L60	959.26 (0.05)	1.04	11.15 (0.05)	0.93
C10-L24	959.34 (0.03)	1.04	11.96 (0.09)	1.00
C10-L48	926.68 (0.03)	1.00	10.63 (0.06)	0.89
C10-L60	924.49 (0.04)	1.00	11.22 (0.07)	0.94

specimens manufactured with type A microfibres, there is a certain confinement of the material, probably due to the effect of the fibres embracing the tensile stresses indirectly induced by compression and containing to some extent the tensile cracking.

Finally, Figure 12 shows the aspect of three representative specimens of each type of fibre at the end of the compression test compared with a mix without fibres. It is worth observing that A type microfibres tend to distribute damage at the whole specimen, producing a very scattered cracking pattern and not producing almost any dust or loose scrap around it. On the contrary, C type specimens tend to concentrate damage along the fibres, inducing spalling and a considerable amount of dust and loose scraps of gypsum around the specimen, although not as much as plain gypsum. As regards B type specimens, although damage tends to be more concentrated than in the case of A type ones, the dust or loose scraps around the specimens are almost non-existent. It is interesting to observe how both, A and B type fibres, show a certain containing effect regarding the material cracking and splitting, but the A type fibres also induce certain confinement in the material that helps to extend the maximum compression strength for larger displacement values, which cannot be observed in specimens made with B type fibres.

4.4. Pull-out test

The pull-out tests have only been carried out with C type fibres, since the micro nature of A type fibres make them difficult to analyse with this test and the B fibres are considered not to provide easily comparable results, given that the ramifications at their endings modify the resistant mechanism which no longer depends only on the fibre-gypsum bonding interface.

Figure 13 displays the load-slip diagrams obtained for three fibre-embedding lengths: 10, 20 and 30 mm. The blue shades represent the experimental envelope for each length and the lines the average diagrams.

In all three cases, the load increases up to a first maximum, then decreases down to a local minimum and continues with increasing-decreasing cycles where the local maximum becomes smaller as the test progresses. The cadence of the local maxima is in all three cases around 2 mm, which suggests that these load oscillations are directly related to the shape pattern of C-type fibres, which is repeated every 2 mm, as can be observed in Figure 1.

The first maximum load increases with the embedding length, as expected, presenting values of around 210, 160 and 110 N for embedding lengths of 30, 20 and 10 mm, respectively. It is interesting and somewhat surprising to see that the first maximum load is for all three embedding lengths similar to those obtained in [34] for cement mortar, a significantly stronger matrix ($\approx$ 225 N for L = 30 mm, $\approx$ 160 N for L = 20 mm and $\approx$ 130 N for L = 10 mm). This suggests that the bonding mechanism of this type of fibres relies mainly on the fibre and not clearly on the strength of the matrix. The explanation for the progressive decay of the local maximum loads is pretty straightforward, since as the fibre is pulled out of the gypsum matrix, a shorter length of fibre remains inside, thus the bonding mechanism becomes weaker. Nevertheless, the first load decay is always significantly higher that the rest in all cases, which could be due to the fact that the

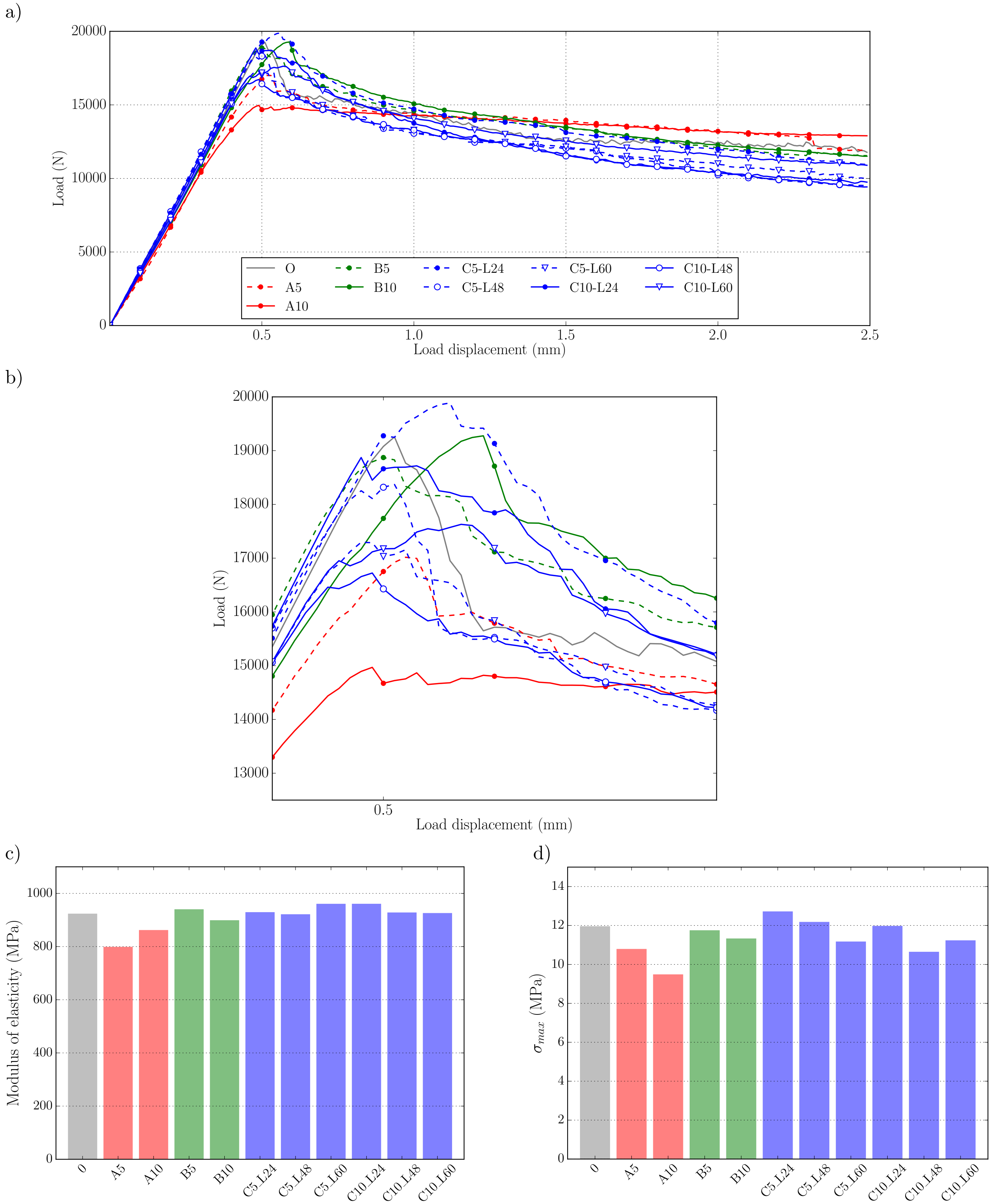

Figure 11: Experimental results of the compression tests: a) load-displacement diagrams, b) detail of the peaks in the load-displacement diagrams, c) average modulus of elasticity and d) average maximum compression stress.

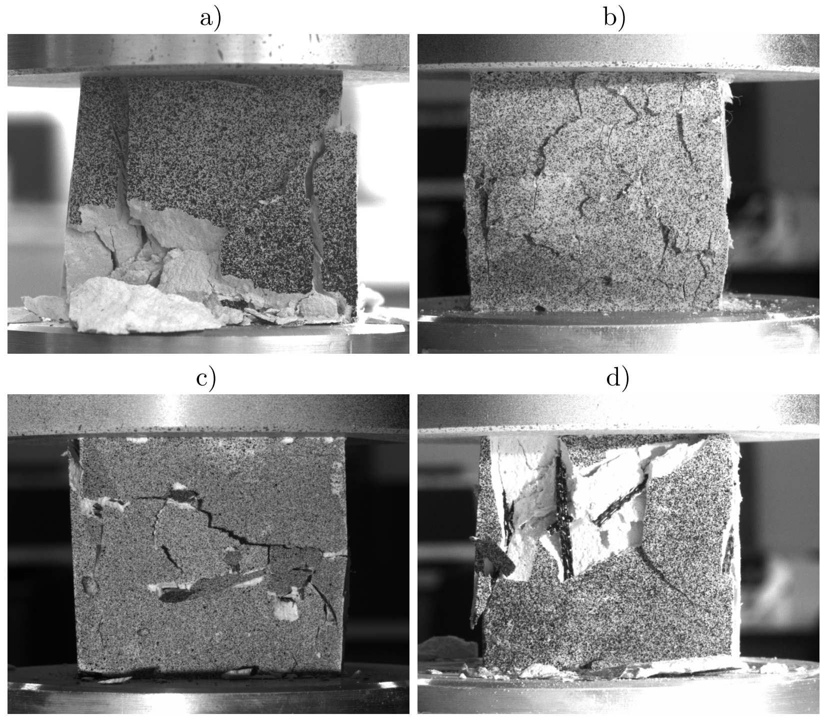

Figure 12: Images of specimens after the compression test is finished: a) 0 type specimen, b) A type specimen, c) B type specimen and d) C type specimen (L=48 mm).

matrix in contact with the fibre is intact at the beginning of the test, but after the first decay, it is slightly polished by the fibre displacement, thus offering smaller resistance to the pulling out of the fibre.

The failure always results from fibre-matrix debonding and slipping, but not from the breakage of the fibre. This is in agreement with the experimental results, where no broken fibre was found, but fibres were always pulled out from gypsum. Longer embedding lengths could lead to different results, but since the maximum fibre length is in this study equal to 60 mm in an ideal case, the maximum embedding length would be 30 mm, which coincides with the maximum length considered in the pull-out test. These results are in accordance with the three-point bending analyses. Given that fibres embedded 30 mm were still pulled-out and did not reach the maximum tensile strength of the fibres, the critical length of this fibre type in gypsum is higher than 30mm. This explains the better results for 60 mm long fibres.

It is worth noting that only the case of fibres oriented parallel to the load direction is considered. The orientation of the fibres with respect to the load direction has a strong influence on this problem, as studied in [34], therefore these results are only a first approximation to the problem and they can be complemented in future research.

5. Conclusions

In this paper the mechanical and fracture behaviour of polymer-fibre reinforced specimens was studied, using micro and macrofibres with different surface finishings and lengths. The main conclusions can be summarised as follows:

- The fibre size has a strong influence on the fresh state of the mix, leading to less workable mixes when microscopic fibres are used. The micro size of the fibres lead to higher amount of water attached to them, thus producing a thicker mix.

- In general, both macrofibres used in this study (B and C) have a better performance in fracture if compared with the microfibres A.

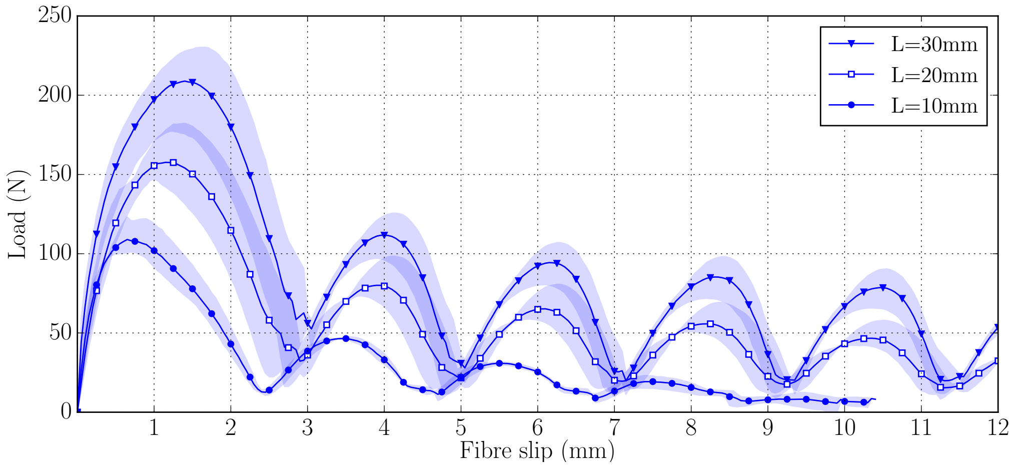

Figure 13: Experimental results of the pull-out tests on specimens manufactured with C fibres

- In the case of the macrofibres, the fibre length is of paramount importance. Since the gypsum matrix is relatively weak, in the case of macrofibres, failure is always the result of the debonding of the fibres and the matrix, therefore, longer fibres provide better performance. When too short fibres are used (L=24mm) the efficiency of the reinforcement is surprisingly low.
- The surface finishing of the macrofibres modifies their fracture behaviour. In the case of the embossed surface fibres (C type), the load displacement diagrams of the three-point bending tests present abrupt load changes related to this issue, while in the case of B type fibres, the diagrams are smooth. The macro nature of B and C fibres tends to concentrate the fibre reinforcement in very specific zones of the specimen, thus greatly improving the mechanical properties in some regions and not affecting others, whereas the micro nature of A fibres strengthen the gypsum matrix in a uniform way.
- The use of embossed surface macrofibres (type C) leads to a distribution of the fracture processes over a wider region in the gypsum matrix, thus smaller values of crack opening, especially in the case of longer fibres (L=60 mm). This type of surface finishing improves the fibre anchorage with the gypsum matrix and makes it more efficient, thus extending their reinforcement to higher values of the load displacement.
- The use of fibres greatly increase the released energy of the material during the fracture process, being remarkably high in the case of relatively long macrofibres (B and C with lengths of 48 and 60 mm).
- Under compression, the use of microfibres slightly reduce the elastic-modulus of the material and the maximum bearing load, which is not observed in the case of specimens manufactured with macrofibres. Microfibres uniformly modify the microstructure of the material at a microscopic scale and can be seen as a new material itself before damage begins. In the case of specimens reinforced with macrofibres, the material behaviour before damage begins is similar to unreinforced gypsum because, at a microscopic scale, the load is born by gypsum itself; fibres only begin to modify the material behaviour when damage begins.
- The use of microfibres seems to induce a certain confinement effect which reduce the load decay after peak in the compression tests.
- Further studies about the fibre orientation factor for the manufacture processes used in FRG could improve the reliability of this material for future applications.
- The results of this study have shown that there is a wide range of possible applications of gypsum reinforced with polymer fibres.

Acknowledgements

The authors gratefully acknowledge the financial support provided by the Ministry of Economy and Competitiveness of Spain through the Research Fund Project BIA2016-78742-C2-2-R. They also wish to thank Sika for providing the fibres used in this study and wish to thank Gabriel Pardo for their valuable comments at the first stages of the experimental work.

References

[1] Zollo RF. Fiber-reinforced concrete: an overview after 30 years of development. Cement and Concrete Composites. 1997;19(2):107 – 122. Available from: http://www.sciencedirect.com/science/article/pii/S0958946596000467.

[2] Banthia N, Gupta R. Influence of polypropylene fiber geometry on plastic shrinkage cracking in concrete. Cement and Concrete Research. 2006;36(7):1263 – 1267. Available from: http://www.sciencedirect.com/science/article/pii/S0008884606000056.

[3] Bentur A, Mindess S. Fibre reinforced cementitious composites. CRC Press; 2014.

[4] Alberti MG, Enfedaque A, Gálvez JC. Comparison between polyolefin fibre reinforced vibrated conventional concrete and self-compacting concrete. Construction and Building Materials. 2015;85:182 – 194. Available from: http://www.sciencedirect.com/science/article/pii/S0950061815002548.

[5] Beverly P. fib model code for concrete structures 2010. Ernst & Sohn; 2013.

[6] DBV, Merkblatt StahlfaserbetonDeutsche Beton Vereins, Guide to Good Practice. German Society for Concrete and Construction Technology; 2001.

[7] CNR-DT 204/2006. Guide for the design and construction of fiber-reinforced concrete structures. Consiglio Nazionale delle Riserche, Rome, Italy; 2006.

[8] EHE-08, Spanish Structural Concrete Code. Spanish Minister of Public Works, Madrid, Spain; 2008.

[9] Alberti MG, Enfedaque A, Gálvez JC, Agrawal V. Reliability of polyolefin fibre reinforced concrete beyond laboratory sizes and construction procedures. Composite Structures. 2016;140:506 – 524. Available from: http://www.sciencedirect.com/science/article/pii/S0263822315011587.

[10] García Santos A. Comportamiento mecánico de yeso reforzado con polímeros sintéticos. Universidad Politécnica de Madrid; 1988.

[11] Santos AG. PPF-reinforced, ESP-lightened gypsum plaster. Materiales de construcción. 2009;59(293):105–124.

[12] del Mar Barbero-Barrera M, Flores-Medina N, Pérez-Villar V. Assessment of thermal performance of gypsum-based composites with revalorized graphite filler. Construction and Building Materials. 2017;142:83–91.

[13] Zhu C, Zhang J, Peng J, Cao W, Liu J. Physical and mechanical properties of gypsum-based composites reinforced with PVA and PP fibers. Construction and Building Materials. 2018;163:695–705.

[14] Medina NF, Barbero-Barrera MM. Mechanical and physical enhancement of gypsum composites through a synergic work of polypropylene fiber and recycled isostatic graphite filler. Construction and Building Materials. 2017;131:165–177.

[15] Dalmay P, Smith A, Chotard T, Sahay-Turner P, Gloaguen V, Krausz P. Properties of cellulosic fibre reinforced plaster: influence of hemp or flax fibres on the properties of set gypsum. Journal of materials science. 2010;45(3):793–803.

[16] Evaluation of bio-degummed hemp fibers as reinforcement in gypsum plaster. Composites Part B: Engineering;.

[17] Iucolano F, Boccarusso L, Langella A. Hemp as eco-friendly substitute of glass fibres for gypsum reinforcement: Impact and flexural behaviour. Composites Part B: Engineering. 2019;175:107073. Available from: http://www.sciencedirect.com/science/article/pii/S135983681931337X.

[18] Behfarnia K, Behravan A. Application of high performance polypropylene fibers in concrete lining of water tunnels. Materials & Design. 2014;55:274–279.

[19] Alberti MG, Enfedaque A, Gálvez JC, Pinillos L. Structural Cast-in-Place Application of Polyolefin Fiber–Reinforced Concrete in a Water Pipeline Supporting Elements. Journal of Pipeline Systems Engineering and Practice. 2017;8(4):05017002.

[20] Enfedaque A, Alberti M, Gálvez J, Rivera M, Simón-Talero J. Can Polyolefin Fibre Reinforced Concrete Improve the Sustainability of a Flyover Bridge? Sustainability. 2018;10(12):4583.

[21] Alberti MG, Gálvez JC, Enfedaque A, Carmona A, Valverde C, Pardo G. Use of Steel and Polyolefin Fibres in the La Canda Tunnels: Applying MIVES for Assessing Sustainability Evaluation. Sustainability. 2018;10(12):4765.

[22] Medina NF, Barbero-Barrera MM. Mechanical and physical enhancement of gypsum composites through a synergic work of polypropylene fiber and recycled isostatic graphite filler. Construction and Building Materials. 2017;131:165 – 177. Available from: http://www.sciencedirect.com/science/article/pii/S0950061816318335.

[23] Zhu C, Zhang J, Peng J, Cao W, Liu J. Physical and mechanical properties of gypsum-based composites reinforced with PVA and PP fibers. Construction and Building Materials. 2018;163:695 – 705. Available from: http://www.sciencedirect.com/science/article/pii/S0950061817325734.

[24] Enfedaque A, Gálvez JC, Suárez F. Analysis of fracture tests of glass fibre reinforced cement (GRC) using digital image correlation. Construction and Building Materials. 2015;75:472 – 487. Available from: http://www.sciencedirect.com/science/article/pii/S0950061814012434.

[25] Lakavath C, Joshi SS, Prakash SS. Investigation of the effect of steel fibers on the shear crack-opening and crack-slip behavior of prestressed concrete beams using digital image correlation. Engineering Structures. 2019;193:28 – 42. Available from: http://www.sciencedirect.com/science/article/pii/S0141029618335880.

[26] UNE-EN 13279-2: Gypsum binders and gypsum plasters - Part 2: Test methods; 2014.

[27] UNE-EN 13279-1: Gypsum binders and gypsum plasters - Part 1: Definitions and requirements; 2009.

[28] Chu T, Ranson W, Sutton MA. Applications of digital-image-correlation techniques to experimental mechanics. Experimental mechanics. 1985;25(3):232–244.

[29] Sutton MA, Orteu JJ, Schreier H. Image correlation for shape, motion and deformation measurements: basic concepts, theory and applications. Springer Science & Business Media; 2009.

[30] Solutions C. Vic-2D. Reference Manual. 2009;.

[31] Schindelin J, Rueden CT, Hiner MC, Eliceiri KW. The ImageJ ecosystem: An open platform for biomedical image analysis. Molecular reproduction and development. 2015;82(7-8):518–529.

[32] Enfedaque A, Alberti MG, Gálvez JC. Influence of Fiber Distribution and Orientation in the Fracture Behavior of Polyolefin Fiber-Reinforced Concrete. Materials. 2019;12(2):220.

[33] Suárez F, Gálvez J, Enfedaque A, Alberti M. Modelling fracture on polyolefin fibre reinforced concrete specimens subjected to mixed-mode loading. Engineering Fracture Mechanics. 2019;211:244–253.

[34] Alberti M, Enfedaque A, Gálvez J, Ferreras A. Pull-out behaviour and interface critical parameters of polyolefin fibres embedded in mortar and self-compacting concrete matrixes. Construction and Building Materials. 2016;112:607–622.

Dear Editor,
Please, find enclosed the revised version of the following paper:

Journal: Construction and Building Materials
Manuscript ID: CONBUILDMAT-D-19-09653
Title: On the fracture behaviour of fibre-reinforced gypsum using micro and macro polymer fibres
Author: F. Suárez, L. Felipe-Sesé, F.A. Díaz, J.C. Gálvez, M.G. Alberti

We would like to sincerely thank the reviewers for their comments, they have helped us correct small but important issues and complete some information, overall improving the quality of the paper. We have found their comments helpful and constructive.

Below we address each of the remarks made by the authors (in blue) to the comments of the reviewers and reference the changes made in the manuscript (highlighted in red font in the new version).

Yours faithfully,

The authors

Comments to reviewers

Reviewer #1

1. The conclusions are limited to reporting observations based on the test results. It will be more meaningful to supplement these observations with appropriate reasoning, wherever possible.
2. Mention may also be made of potential applications of the different FRGs adopted in the testing.

We have included additional observations in the some conclusions, that have been extended as follows (bold font highlights the text added):

- *"The surface finishing of the macrofibres modifies their fracture behaviour. In the case of the embossed surface fibres (C type), the load displacement diagrams of the three-point bending tests present abrupt load changes related to this issue, while in the case of B type fibres, the diagrams are smooth.* ***The macro nature of B and C fibres tends to concentrate the fibre reinforcement in very specific zones of the specimen, thus greatly improving the mechanical properties in some regions and not affecting others, whereas the micro nature of A fibres strengthen the gypsum matrix in a uniform way.***
- *The use of embossed surface macrofibres (type C) leads to a distribution of the fracture processes over a wider region in the gypsum matrix, thus smaller values of crack opening, especially in the case of longer fibres (L=60 mm).* ***This type of surface finishing improves the fibre anchorage with the gypsum matrix and makes it more efficient, thus extending their reinforcement to higher values of the load displacement.***
  (...)
- *Under compression, the use of microfibres slightly reduce the elastic-modulus of the material and the maximum bearing load, which is not observed in the case of specimens manufactured with macrofibres.* ***Microfibres uniformly modify the microstructure of the material at a microscopic scale and can be seen as a new material itself before damage begins. In the case of specimens reinforced with macrofibres, the material behaviour before damage begins is similar to unreinforced gypsum because, at a microscopic scale, the load is born by gypsum***

itself; fibres only begin to modify the material behaviour when damage begins."

Reviewer #2

General comments

The paper deals with an interesting and widely discussed topic, the use of fibers to reinforce a largely used building material, such as gypsum.

Overall, the manuscript is well written and organized; nevertheless, the following minor revisions are addressed to the authors, in order to improve the paper and to consider it for publication.

- The "Introduction Section" should be improved and better discussed. In particular, some references are too old (Refs [1], [8]), and in some cases the use of a European Standard should be cited instead of a National Standard (Ref [5]).

Moreover, the state of the art presented in this Section mainly deals with polymeric fibers, while no discussions are furnished about other fibers typologies widely proposed as building materials reinforcements. In particular, nowadays many studies deal with the use of cellulosic fibers as reinforcement of gypsum plasters. In this aim, I suggest to the authors to consider some of the following papers, both to improve the Introduction Section and to compare the mechanical behaviour observed in the manuscript with some behaviour reported in literature:

- Iucolano F. et al, "Evaluation of Bio-Degummed Hemp Fibers as Reinforcement in Gypsum Plaster", COMPOSITES PART B (2018), 138: 149-156.
- Dalmay P. et al., "Properties of cellulosic fibre reinforced plaster: influence of hemp or flax fibres on the properties of set gypsum", J Mater Sci (2010) 45:793-803.
- Iucolano F. et al., "Hemp as eco-friendly substitute of glass fibres for gypsum reinforcement: impact and flexural behaviour", COMPOSITES PART B (2019), 175, 107073.

We agree that some references are old, but regarding polymeric fibres used as reinforcement in gypsum, which is the main topic covered in this manuscript, the work by García-Santos is, in our opinion, a good reference and must be included.

In the manuscript we only deal with polymeric fibres, that is why in the introduction not much information was given about natural fibres. In any case, we have followed this recommendation and extended the introduction, including the references and mentioning the interest of using natural fibres, such as hemp or flax, as reinforcement in gypsum. This way, we think we focus the introduction on the polymeric fibres but also mention current trends in FRG:

"...The use of natural fibres, such as hemp or flax, is also appealing, since they can improve the mechanical, acoustic and thermal properties of gypsum in an eco-friendly manner [15, 16, 17]..."

- In Table 1, the authors indicate that the gypsum to water ratio (g/w) used to manufacture all the specimens is equal to 0.63, that means a w/g ratio about 1.6. In my opinion this ratio involves in a too high amount of water in the mixture, as in literature are reported w/g ratios mainly belonging to the range 0.7-1.0 (e.g. see the above-suggested papers). The authors should clarify this item.

Thank you very much for this remark. The value is, in fact, the gypsum/water ratio, not the water/gypsum ratio. We have corrected this issue in Table 1.

In addition to this, it is true that we had not provided information about why the g/w ratio employed here is 0.63. This ratio was obtained using the procedure described in the standard, several experiments were carried out until two of them strictly met the standard requirements (in terms of timing and rate of gypsum adding) We have included the following text at the last paragraph of section 2:

"...Regarding the amount of water added in each mix, the gypsum to water ratio (w/g) was obtained following the procedure described in the standard [26], which determines the mass of gypsum that can be saturated when it is sprinkled into 100 g of water..."

- In 4.1 paragraph (Fresh state workability) the authors state: "when microfibers A were used, the mix became much thicker" and this behaviour is justified taking into account "the higher amount of water absorbed by these fibers". In my opinion this is a weak explanation, because on the whole polypropylene shouldn't absorb water, and in particular, within the data sheet of Sikafiber M-12 is clearly indicated : "Absorcion de aqua : nula"! Therefore, the different workability of the mixture manufactured with A fibers should be better discussed.

The reviewer is right, the text was misleading and not correct. It is true that, as the Sikafiber M-12 states, the fibres cannot absorb water, since no water penetrates the fibres. What we meant was that, due to the higher specific surface area of these fibres, the amount of water that can be placed on them is significantly higher, thus affecting the workability of the mix. The text has been modified in section 4.1 and in the first conclusion:

"...the microscopic nature of this fibre leads to a higher specific surface area, thus leading to a higher amount of water attached to them..."
"...The micro size of the fibres lead to higher amount of water attached to the them, thus producing a thicker mix..."

- Table 3 reports an interesting comparison between CMOD and load displacement at <delta>=5mm. These CMOD values, however, could be evaluated also from the figures 5 to 7 (right side), if the x-axis scale was higher than 5 mm. Please, consider the possibility to enlarge the x-axis scale of Load/CMOD graphs, to better evaluating the CMOD values in correspondence of a load displacement equal to 5 mm.

The graphs on the right of Figures 5 to 7 have been modified and now show the evolution of the diagrams up to CMOD=8.5mm. Therefore, it is possible to compare the results obtained using the load displacement and the CMOD; this comparison is carried out in Table 3 for a load displacement of delta=5mm.

- Concerning the experimental results of the compression tests, there are no indications about the standard deviations of both maximum compression stress and modulus of elasticity. Please, provide some details on this item.

The relative standard deviations (or coefficients of variation = standard deviation / average) have been included in brackets in Table 4. In addition to this, and thanks to this remark, we have observed a mistake in this table, since some mixes were not named in the right order (affecting mixes C5-L48, C5-L60, C10-L24 and C10-L48). We have carefully checked all the experimental data and have confirmed that this mistake was only present in this table, all the other tables and graphs were correct in the first draft.

- In Table 2, the brackets (N·m) should be substituted with (N·mm).

The reviewer is right, this units were wrong. Anyway, in the new revised version of the manuscript, Table 2 now expresses the energy values in N/m, as explained in the final comment at the end of this document.

- The English language should be revised in the following parts:
- Pag 2, line 37: I suggest to change "has proved to provide" with "has provided";
- Pag 4, line 100: the term "employinga" should be changed with "employing";
- Pag 5, line 128: the term "identying" should be changed with "identifying";
- Pag 6, lines 144 and 146: the term "ammount" should be changed with "amount";
- Pag 9, line 200: the term "gysum" should be changed with "gypsum".

Thank you for these corrections; they have been amended in the new version of the manuscript.

Final comment

As a final comment, we would like to say that we have decided to modify the way the released energy is expressed in Table 2. In the first draft, these energy values were expressed in N·mm and referred to the measured energy in a test. In the revised version, we have expressed these values as (Released energy / fracture surface area), thus given in N/m. For example, since the notch is of 13 mm and the specimen height width are both equal to 40 mm, the fracture surface area is: (40-13)*40 = 1080 mm^2. Therefore, for example, the released energy of mix 0, which was in the first draft equal to 25.89 N·mm is now:

$$25.89\ N\cdot mm/1080\ mm^2 = 0.02397\ N/mm = 23.97\ N/m$$

The reason of this change is that, in this form, the results can be easily compared with other tests carried out with different geometries (of notch and specimen).

*Highlights

Highlights

- Performance of different polymer fibers as reinforcement of gypsum is studied.
- Three-point bending, compression and pull-out tests are employed for characterising the mixes.
- The use of Digital Image Correlation has proved to be very helpful with the aforementioned tests.
- The macro or micro nature of the fibres modifies the fracture mechanisms involved.

Graphical Abstract

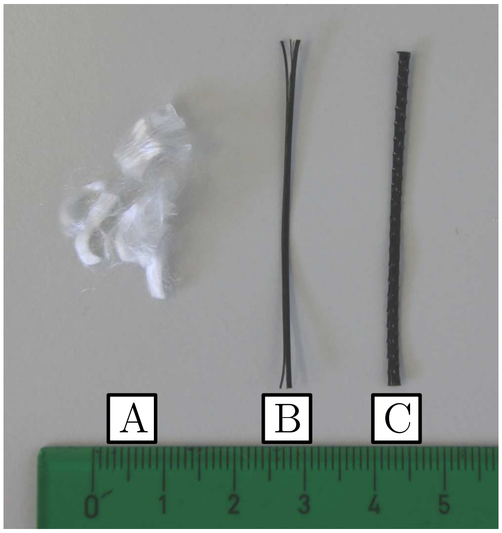

Mix	g/w	A fibres	B fibres	C fibres		
				L=24 mm	L=48 mm	L=60 mm
0	0.63	–	–	–	–	–
A5	0.63	5	–	–	–	–
A10	0.63	10	–	–	–	–
B5	0.63	–	5	–	–	–
B10	0.63	–	10	–	–	–
C5-L24	0.63	–	–	5	–	–
C10-L24	0.63	–	–	10	–	–
C5-L48	0.63	–	–	–	5	–
C10-L48	0.63	–	–	–	10	–
C5-L60	0.63	–	–	–	–	5
C10-L60	0.63	–	–	–	–	10

Polymer fibres **Fibre-reinforced gypsum mixes**

Three-point bending test

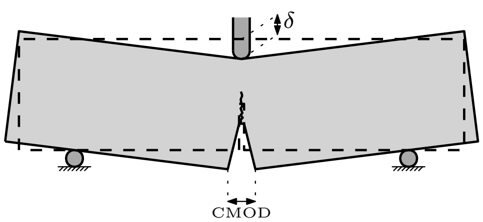

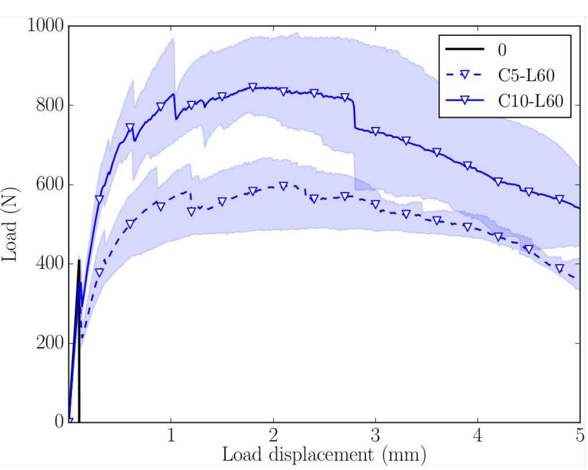

Compression test

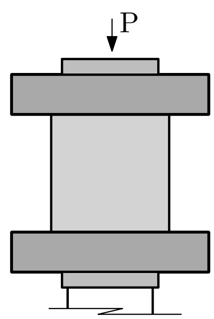

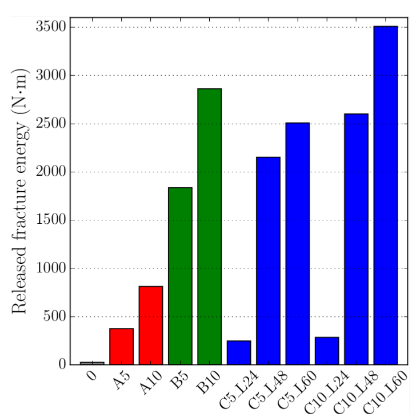

Pull-out test

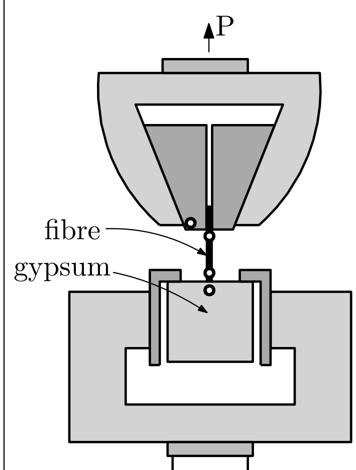

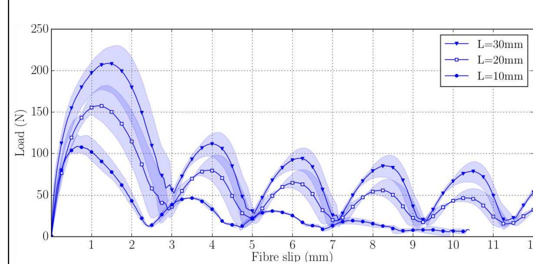

LaTeX Source Files
Click here to download LaTeX Source Files: Latex_source_files.zip

***Declaration of Interest Statement**

Declaration of interests

☒ The authors declare that they have no known competing financial interests or personal relationships that could have appeared to influence the work reported in this paper.

☐The authors declare the following financial interests/personal relationships which may be considered as potential competing interests:

*Credit Author Statement

Author contribution statement

- Conceptualization: F. Suárez, M.G. Alberti and J.C. Gálvez.
- Funding acquisition: F.A. Díaz and F. Suárez.
- Investigation: F. Suárez and L. Felipe-Sesé.
- Methodology: F. Suárez, L. Felipe-Sesé and M.G. Alberti.
- Resources: F.A. Díaz and L. Felipe-Sesé.
- Supervision: F. Suárez and L. Felipe-Sesé.
- Validation: F.A. Díaz, M.G. Alberti and J.C. Gálvez.
- Original draft: F. Suárez.
- Review and editing: F.A. Díaz, L. Felipe-Sesé, M.G. Alberti and J.C. Gálvez.

*Title page

On the fracture behaviour of fibre-reinforced gypsum using micro and macro polymer fibres

F. Suárez[a], L. Felipe-Sesé[a], F.A. Díaz[b], J.C. Gálvez[c], M.G. Alberti[c]

[a] *Departamento de Ingeniería Mecánica y Minera. Universidad de Jaén. Campus Científico-Tecnológico de Linares. Cinturón Sur 23700 – Linares (Jaén), Spain*
[b] *Departamento de Ingeniería Mecánica y Minera. Universidad de Jaén. Campus Las Lagunillas. 23071 – Jaén, Spain*
[c] *Departamento de Ingeniería Civil-Construcción. Universidad Politécnica de Madrid . E.T.S.I. Caminos, Canales y Puertos, C/ Profesor Aranguren s/n 28040 – Madrid, Spain*

- Corresponding author: F. Suárez.
- E-mail addresses: fsuarez@ujaen.es, lfelipe@ujaen.es, fdiaz@ujaen.es, jaime.galvez@upm.es, marcos.garcia@upm.es

*Revised manuscript with changes marked

On the fracture behaviour of fibre-reinforced gypsum using micro and macro polymer fibres

F. Suárez[a], L. Felipe-Sesé[a], F.A. Díaz[b], J.C. Gálvez[c], M.G. Alberti[c]

[a]*Departamento de Ingeniería Mecánica y Minera. Universidad de Jaén. Campus Científico-Tecnológico de Linares. Cinturón Sur 23700 – Linares (Jaén), Spain*
[b]*Departamento de Ingeniería Mecánica y Minera. Universidad de Jaén. Campus Las Lagunillas. 23071 – Jaén, Spain*
[c]*Departamento de Ingeniería Civil-Construcción. Universidad Politécnica de Madrid . E.T.S.I. Caminos, Canales y Puertos, C/ Profesor Aranguren s/n 28040 – Madrid, Spain*

Abstract

Gypsum is the most widely used material as interior lining in buildings due to its low cost and good habitability conditions. The use of fibres as randomly distributed reinforcement of quasibrittle matrices, such as gypsum, remarkably improve the material behaviour under tensile stresses. In this work, the fracture behaviour of gypsum specimens reinforced with several types of polymer fibres was assessed, for one of them three fibre lengths were studied. Three types of polymer fibres were employed, with one of them being of microscopic scale and the other two of macroscopic scale. The mechanical behaviour of each mix was studied by means of three-point bending tests and compression tests that were analysed using a digital image correlation system. To study the influence of the fibre length, pull-out tests were also performed. The size, surface finishing and length of the fibres strongly affect the material properties and the way that the fracture mechanisms are developed.

Keywords: Fibre-reinforced gypsum, Polyolefin fibres, Fracture.

1. Introduction

Due to its low cost as well as good habitability and comfort conditions, gypsum is the most extended material as interior lining in buildings. In the last decades, this industry has developed new solutions, such as sandwich panels of laminated gypsum or the use of cellulose as reinforcement. On another note, the addition of polymer fibres as reinforcement of quasi-fragile matrices greatly improves the behaviour of the base material, making them suitable for new uses. This reinforcement improves the ductility of the material and increases the fracture energy that the material can absorb before completely losing their load-bearing capacity. This aspect is of particular interest in elements that can experience impact loading or seismic effects, and it has been adopted and studied in the last years in the field of concrete [1, 2, 3, 4]. The Model Code for Concrete Structures [5], as well as other structural concrete standards [6, 7, 8], already include guidelines for the use of fibres as structural reinforcement in concrete. Nevertheless, although this normative seems to reproduce well elements reinforced with steel fibres, there is not enough confidence when other types of fibres are adopted [9].

There are studies about the mechanical properties of fibre reinforced gypsum (FRG) as those by García-Santos [10, 11], which studied the mechanical properties of gypsum reinforced with several types of polymer fibres. Nowadays, the study of how different additions affect the properties of gypsum is still of interest, since in some cases the thermal properties can be enhanced [12] and in other cases the mechanical properties improved [13, 14]. The use of natural fibres, such as hemp or flax, is also appealing, since they can improve the mechanical, acoustic and thermal properties of gypsum in an eco-friendly manner [15, 16, 17]. In any case, the addition of fibres in matrices with low strength under tension, such as concrete or gypsum, usually induces

*F. Suárez
Email address: fsuarez@ujaen.es (F. Suárez)

a better mechanical behaviour that can extend their use to other areas. This has been recently observed with polyolefin fibre reinforced concrete (PFRC), which has already been used as the only reinforcement in structural concrete [18, 19, 20, 21].

When the mechanical properties of FRG have been studied, the mechanical tests were usually reduced to obtaining the compression strength, the elastic modulus and the flexural strength [10, 22, 23]. However, the fracture energy absorbed by the material before completely losing its load-bearing capacity is of significant importance in some cases. It is a key enhancement of FRG when compared with plain gypsum. This material property should also be taken into account for characterising the performance of the material.

In this work, the mechanical properties of FRG specimens, made with several types of polymer fibres, were studied. Three types of polymer fibres were considered, with one of them being micro and the other two macro. Each of these fibres were mixed with gypsum using two proportions, 5 and 10 kg/m^3, and in the case of one of the macrofibres, three lengths were used: 24, 48 and 60 mm. The study was performed by testing specimens under compression and under a three-point bending test on notched specimens, which also provides information about the fracture energy released by the material before the specimen collapses. Finally, in the case of one of the macrofibres, pull-out tests were performed in order to explain some remarkable differences observed in the flexural behaviour of specimens made with this type of fibres but using different fibre lengths. As discussed below, the pull-out test is only carried out with one type of the macro-fibres used in this study, given that for reasons that will be explained later, the use of this test with the other fibres make the results hard to analyse.

The use of a digital image correlation system (DIC) has provided interesting information about how the fibres modify the fracture mechanisms of quasibrittle materials [24, 25]. In this study, it allowed keeping track of certain parameters in the three-point bending test and obtaining the complete strain field on the specimens surface, which helped to identify how the use of different types of fibres modified the fracture behaviour of the material.

2. Design of the study

The main aim of this study was to analyse the behaviour of FRG when polymer fibres of different size scales were employed. To do this, three types of fibres were selected, one of them being of microscopic size and two of them being macroscopic, identifying the microscopic fibres with letter A and the two macroscopic fibres with letters B and C, as shown in Figure 1. In the case of the microscopic fibre, it resembles short textile fibres gathered in small bundles. Both macroscopic fibres are made of the same polymer but have different shapes and surface finishing. In the case of fibre B, the fibre surface is mainly smooth and the endings show ramifications, while the surface of C fibres is embossed and no ramifications can be observed at the endings

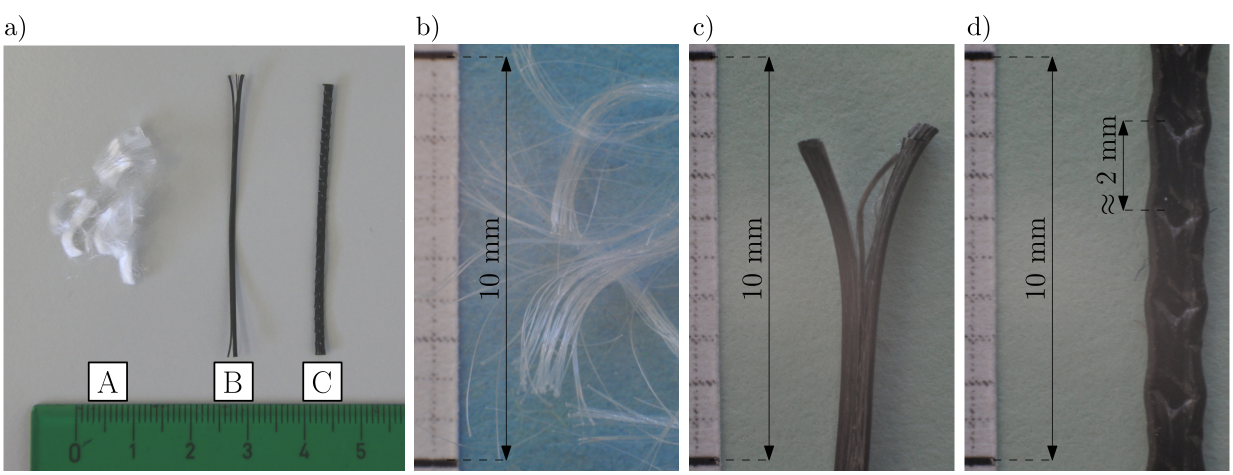

Figure 1: Fibres used in this study: a) General view and nomenclature, b) detail of A type fibres, c) detail of ending in B type fibres and d) detail of the embossed surface of C type fibres.

This study analysed the following aspects regarding polymer fibre reinforcement of gypsum:

Table 1: Gypsum mix proportions (fibre proportions expressed in kg/m^3)

Mix	w/g	A fibres	B fibres	C fibres		
				L=24 mm	L=48 mm	L=60 mm
0	0.63	–	–	–	–	–
A5	0.63	5	–	–	–	–
A10	0.63	10	–	–	–	–
B5	0.63	–	5	–	–	–
B10	0.63	–	10	–	–	–
C5-L24	0.63	–	–	5	–	–
C10-L24	0.63	–	–	10	–	–
C5-L48	0.63	–	–	–	5	–
C10-L48	0.63	–	–	–	10	–
C5-L60	0.63	–	–	–	–	5
C10-L60	0.63	–	–	–	–	10

- Difference on the mechanical properties of FRG mixes made using micro and macro polymer fibres.
- Difference on the behaviour of FRG mixes using macro fibres with different surface finishing.
- Influence on the fibre proportion on the mechanical properties for each of the fibres considered in the study.
- Influence of the fibre length when using polymer macro-fibres.

Therefore, 11 sets of three specimens each were prepared, one of plain gypsum with no fibres added, which will serve as reference (0), two with microscopic A fibres employing fibre dosages of 5 and 10 kg/m^3 (A5 and A10), two with macroscopic B fibres employing the same fibre dosages mentioned (B5 and B10) and six with macroscopic C fibres combining the two mentioned fibre dosages and three fibre lengths of 24, 48 and 60 mm (C5-L24, C5-L48, C5-L60, C10-L24, C10-L48 and C10-L60). Regarding the amount of water added in each mix, the water to gypsum ratio (w/g) was obtained following the procedure described in the standard [26], which determines the mass of gypsum that can be saturated when it is sprinkled into 100 g of water. Table 1 summarises this information.

3. Experimental work

This section presents the materials used for manufacturing the various sets of specimens described above and the experimental tests carried out, including a description of the experimental setups and tools used.

3.1. Materials and mixes

Gypsum

Selected gypsum corresponds to plaster, classified as A1 according to the EN 13279-1 standard [27], composed by hemihydrated calcium sulphate ($CaSO_4 \cdot 0.5\ H_2O$). This material is commonly used for manufacturing precast elements such as plasterboard panels used in sandwich-type partitions.

Fibres

Three types of fibres were used in this study, they can be seen in Figure 1. Fibres A are polypropylene microfibres, named Sikafiber M-12, that are usually employed in concrete and mortars for reducing their cracking and increasing their durability. They are 12 mm long and have a diameter of 31 μm. Fibres B are polyolefin macrofibres with a length of 48 mm, equivalent diameter of 0.92 mm and smooth finishing surface, presenting ramifications at their endings. Finally, C-type fibres are also polyolefin macrofibres, but their aspect is different from B-type fibres, they are thicker and their surface is embossed with a pattern that repeats every 2 mm along them (a more detailed description can be found in [4]). Regarding C-type fibres, three lengths are used: 24, 48 and 60 mm.

3.2. Specimens

Sets of three 160×40×40 mm^3 prismatic specimens of each gypsum mix were manufactured following a slight variation of the procedure described in UNE-EN 13279-2 [26] for adding the fibres. Such procedure is described below:

1. Gypsum was poured on the water and manually mixed for 40 seconds.
2. Fibres were added and mixed manually for 20 seconds.
3. Mixing continued for 60 more seconds in a planetary mixer at low speed.
4. Moulds, previously impregnated with release agent, were filled.
5. Moulds were hit to eliminate air bubbles and finally levelled.
6. The specimens were unmoulded and cured inside a controlled-climate chamber for seven days at 23±2^{o}C and relative humidity of 50±5%.
7. Specimens were dried inside an oven at 50^{o}C for 48 hours.
8. Specimens were cooled at room temperature and the notch was cut with a band saw by dry way.
9. Specimens were marked with black spray for the later use of digital image correlation (DIC).

3.3. Digital image correlation (DIC)

A digital image correlation system was used to measure strains in the three-point bending tests and the compression tests. This technique is based on comparing images of a specimen obtained during a test with the initial unloaded image of the specimen; this comparison allows obtaining the displacement field on a desired region of the specimen, thus, the derived strain field can be easily obtained. For more information on this technique, the reader can consult [28, 29]. In this work an Allied Stingray F-080C with a resolution of 1032×766 pixels was used and the software Vic-2D, by Correlated Solutions, was employed [30]. Digital image correlation in 2D was performed by employing a 21 pixels size facet and 5 pixels of step.

3.4. Experimental setup of the three-point bending test

Figure 3a shows a scheme of this test. In this study the span length was $L = 100$ mm, the specimen height $h = 40$ mm and the notch length $a = 13$ mm. Therefore, a span/height relation of 2.5 and a notch of 1/3 the height of the specimen have been considered. The tests were carried out with a dual column testing system of Instron of the 5960 series and using a load cell of 30 kN of capacity. For these tests, the specimens were placed over two cylindrical rolls supported by a horizontal beam and the load was vertically applied, as shown in Figure 3b. The load was applied at low speed (0.05 mm/min) up to the first load decay, in order to reduce the dynamic effect of such a load drop to a minimum, and 0.25 mm/min later. The duration of the test was of 27 minutes for each specimen and images for DIC were capture every 5 seconds.

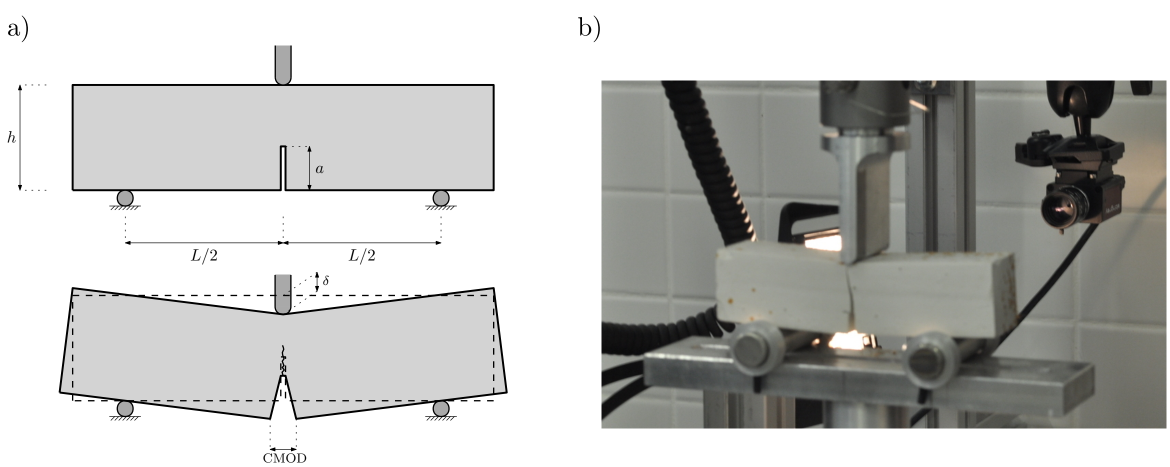

Figure 2: Experimental setup of the three-point bending test on a notched specimen: a) specimen dimensions and displacement parameters; b) experimental setup arranged for the use of DIC.

3.5. Experimental setup of the compression test

After the three-point bending test was carried out, the specimens were cut using a band saw by dry way, obtaining two 40 mm side cubic samples out of each prismatic specimen. These tests were performed following the UNE-EN 13279-2 standard [26], placing each specimen between two cylindrical plates and using the same testing equipment described for the three-point bending tests. The load was applied at a speed of 1 mm/min up to a total displacement of 3 mm and the images for DIC were captured every second.

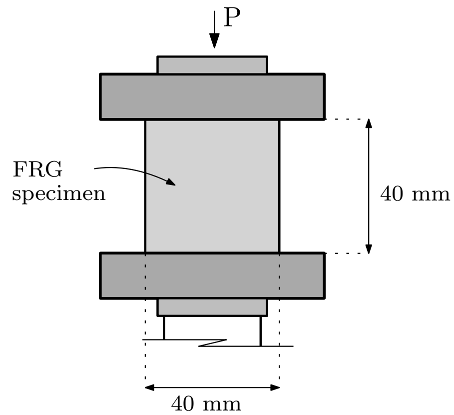

Figure 3: Experimental setup and dimensions of the compression test.

3.6. Experimental setup of the pull-out test

The pull-out allows assessing the quality of the bonding mechanism between the fibres and the matrix in a composite material. In this study, the specimens were manufactured by embedding a fibre up to a certain length inside fresh gypsum, then the standard process of curing and drying described before was applied.

The test consists of pulling a fibre out of the gypsum matrix to obtain a load-slip diagram that identifies the load bearing capacity of the fibre-matrix bonding and how it evolves as the fibre is progressively extracted from the matrix. Figure 4 shows a scheme of the test (a) and images of one of the test at different stages (b). Apart from the displacement due to the fibre being pulled out of the gypsum matrix, the displacement of the grip may cause slipping between the clamping jaws and the fibre, which would make the displacement measure invalid or not correct. To detect this possible problem and easily identify the tests that must be discarded, four tracking points were attached, one on the clamping jaws, one on the top region of the fibre, one on the bottom part of the fibre and, finally, another one on the gypsum block. The first two allow identifying a possible slipping between the jaws and the fibre and the last two allow measuring the true pull-out displacement during the test. To measure the displacement of each of these points, the ImageJ software [31] was used, which allows precise and easy tracking of the target points. This test was carried out with a load displacement of 1.2 mm/min and capturing one image per second.

4. Results and discussion

This section presents the experimental results. In order to make them easier to read, the results corresponding to plain gypsum (O) are shown in black, those corresponding to polypropylene microfibres (A) are shown in red, those of type B macrofibres are shown in green and those of type C macrofibres are shown in blue. Different fibre dosages and different fibre lengths in the case of B fibres are conveniently identified and marked in each graph.

4.1. Fresh state workability

Although no specific test was carried out to measure the workability of the mixes, significant differences were found in this aspect when using micro or macrofibres. When macrofibres B or C were employed, the workability of the mix in fresh state was good with the fibre proportions analysed (5 and 10 kg/m^3). When microfibres A were used, the mix became much thicker, which was particularly noticeable with the higher

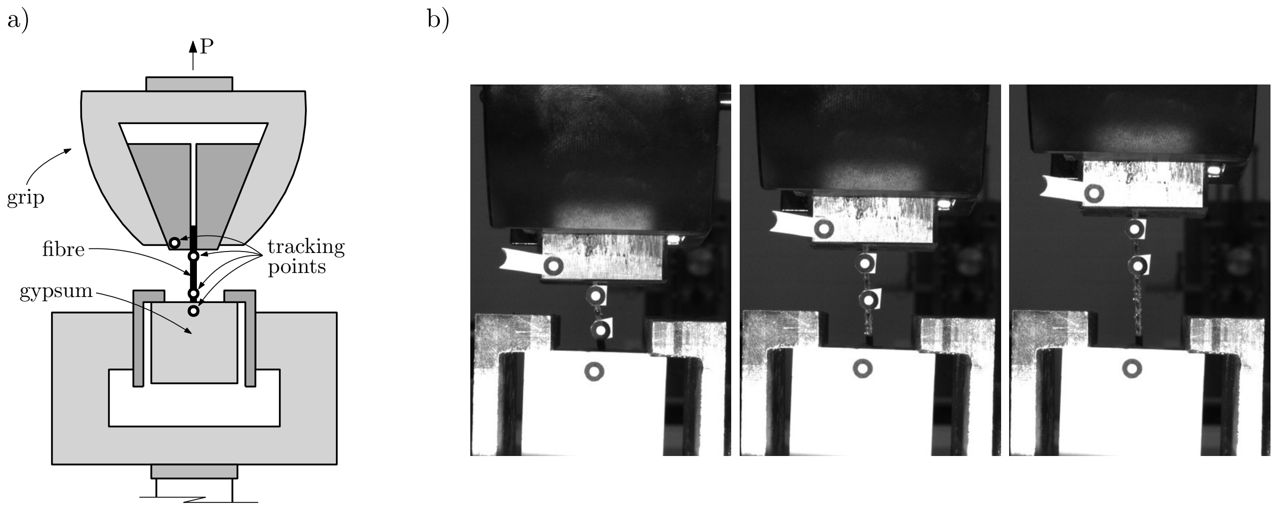

Figure 4: Experimental setup of the pull-out test a) scheme of the setup and b) images of a pull-out test at different instants.

fibre proportion. This was expected, since the microscopic nature of this fibre leads to a higher specific surface area, thus leading to a higher amount of water attached to them. Nevertheless, this suggests that in the case of B or C fibres, higher fibre proportions could be added, but in the case of A fibres, the amount of fibres that can be added is clearly limited by the workability of the mix.

4.2. Three-point bending test

Figures 5, 6 and 7 show the diagrams experimentally obtained for specimens with A, B and C fibres, respectively, using three specimens with each mix. On the left of each figure, the load-displacement diagram is shown and, on the right, the load-CMOD diagram is presented, with CMOD being the crack mouth opening displacement obtained with DIC. In all cases, the results obtained for each fibre dosage, 5 and 10 kg/m^3, are presented together, showing the experimental envelope for each as a shade and the average results (of three specimens) of each dosage with different line styles (dashed for 5 kg/m^3 and continuous for 10 kg/m^3). The average result of plain gypsum (O) is also included in the load-displacement diagrams as a continuous black line, although it is barely visible given that it only develops in the very first instants of the test; as for the load-CMOD diagrams, it is not included, since it would not be visible at all.

Looking at Figure 5, it can be observed that polypropilene microfibres extend the flexural behaviour of gypsum, which becomes remarkably ductile. Unlike plain gypsum, those specimens reinforced with fibre A showed a load recovery after the first load peak, extending the specimen flexural strength beyond 5 mm of load displacement. The first load peak identifies the moment at which the gypsum matrix failed and the fibres became the main mechanism of resistance. The energy released by this fracture process is much higher than in the case of plain gypsum, that shows an almost negligible absorbed energy before losing its load-bearing capacity. When 5 kg/m^3 were added, the enhancement is clearly observed and when 10 kg/m^3 were added, the post-peak strength becomes approximately twice as higher. It is worth noting that the diagrams are smooth, not showing abrupt load changes during the fracture processes.

As regards those specimens manufactured with B macrofibres, Figure 6 shows an analogous behaviour as that observed for specimens manufactured with A microfibres. There was also an important load recovery after the first peak that gradually reached a new maximum and slowly lost its load-bearing capacity. Those specimens with 10 kg/m^3 also showed a higher load-bearing capacity after the first peak compared with those with 5 kg/m^3, although not being as much as twice their maximum recovery load. It is interesting to observe two main differences with regard to the specimens made with A fibres: the load-bearing capacity after the first peak is remarkably high, even leading to a maximum load recovery higher than the first peak, and the experimental repetitiveness in the case of B fibres was significantly lower.

Figure 7 shows the diagrams for all the specimens manufactured with C macrofibres, that is to say, a total of 18 specimens, three per mix. One of the main differences that can be observed concerns the remarkable improvement in the flexural behaviour that was obtained just by modifying the fibre length. When fibres were 24 mm long, the specimens showed a very limited load recovery after the first peak if their behaviour is compared with those obtained with 48 and 60 mm long fibres. The same proportion of fibres with shorter length of these implied a higher number of fibres in the fracture surface of the specimen, which increased the probability of finding more fibres in the crack path, thus a better behaviour could be expected, nevertheless, the experimental results showed a poorer performance when 24 mm fibres were used. It is also interesting to observe that if the results with 48 and 60 mm long fibres are compared, the behaviour is quite similar, even reaching slightly higher recovery loads after peak-load with the latter. Using longer fibres imply fewer fibres in the specimen, therefore, a lower number of fibres crossing the crack path is expected; nevertheless, the experimental results show that it can be beneficial to use longer fibres, even if that reduces the number of them in the mix. Regarding the overall aspect of the diagrams, and not taking into account those of 24 mm long fibres, which are not able to show the load-bearing capacity of this type of fibres, it is interesting to observe that the experimental scatter was very high and that the diagrams showed very often abrupt load changes, which is related to fibres losing their grip with gypsum, thus leading to discrete load drops. It is also worth noting that the longer the fibre, the maximum load after the first peak was observed, taking place at around $\delta = 0.5$ mm in the case of 24 mm long fibres, at around $\delta = 1.75$ mm with 48 long fibres and at around $\delta = 2$ mm with 60 mm long fibres. This agrees with the observations made for polyolefin fibre reinfoced concrete in [32] and [33]. It should be mentioned that the better orientation factor expected for the longer fibres given the relation fibre length/specimen size explains this enhancements proportional with the fibre length and could be considered as expected.

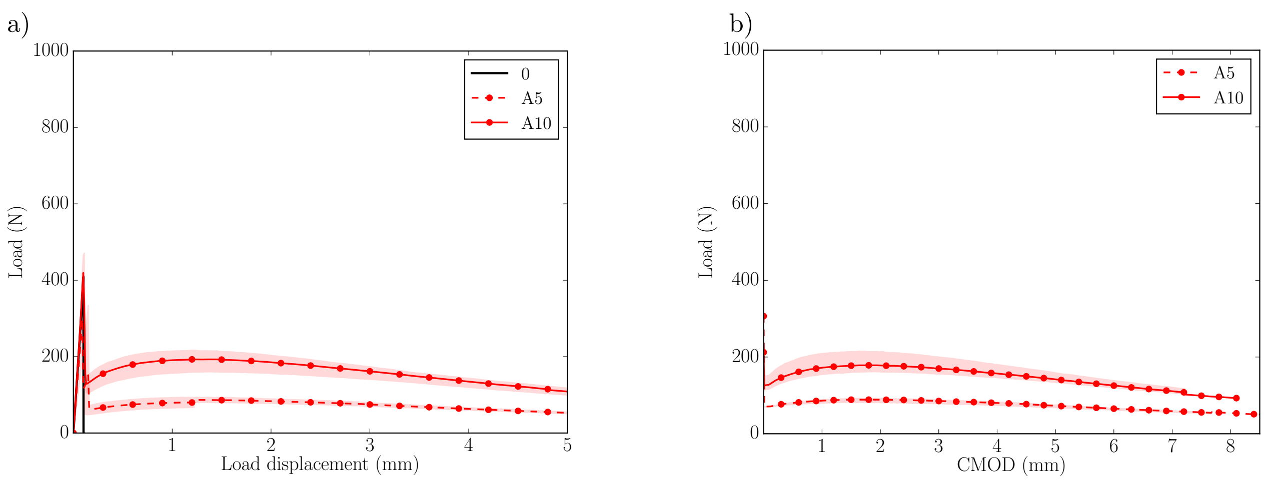

Figure 5: Experimental results of the three-point bending tests on specimens manufactured with A fibres (shaded areas represent the experimental envelopes).

In order to measure the energy released by each mix and compare their performance, this value has been measured for each at three instants of the test corresponding to load displacements of 1, 3 and 5 mm. These values of the specific fracture energy are obtained by computing the area below the curves in the load-load displacement diagrams presented before up to the corresponding value of the considered load displacement and dividing it by the area of the fracture surface, which in this case is a 27 mm×40 mm rectangle. Table 2 lists these values, which are graphically shown in Figure 8. Regarding the reference mix of plain gypsum, O, the value is equal for all the values of δ, since once the maximum load peak is reached, no additional energy is absorbed by the specimen. Regarding those specimens manufactured with any type of fibres, the specific fracture energy increases with δ, although significant differences may be remarked. In the case of the specimens made with the microfibres (A5 and A10) and the specimens made with short C macrofibres (C5-L24 and C10-L24), the energy increase is quite limited; in the case of the former it seems that this performance could be enhanced by increasing the fibre dosage, since the energy is about twice in the case of A10 with respect to A5. Conversely, in the case of the specimens made with 24 mm long C fibres, the fibre dosage does not seem to boost this value.

As for the rest of the fibres, B macrofibres and 48 and 60 mm long C macrofibres, the specific fracture energy is very significant, even leading to high values of more than 100 times those of plain gypsum when

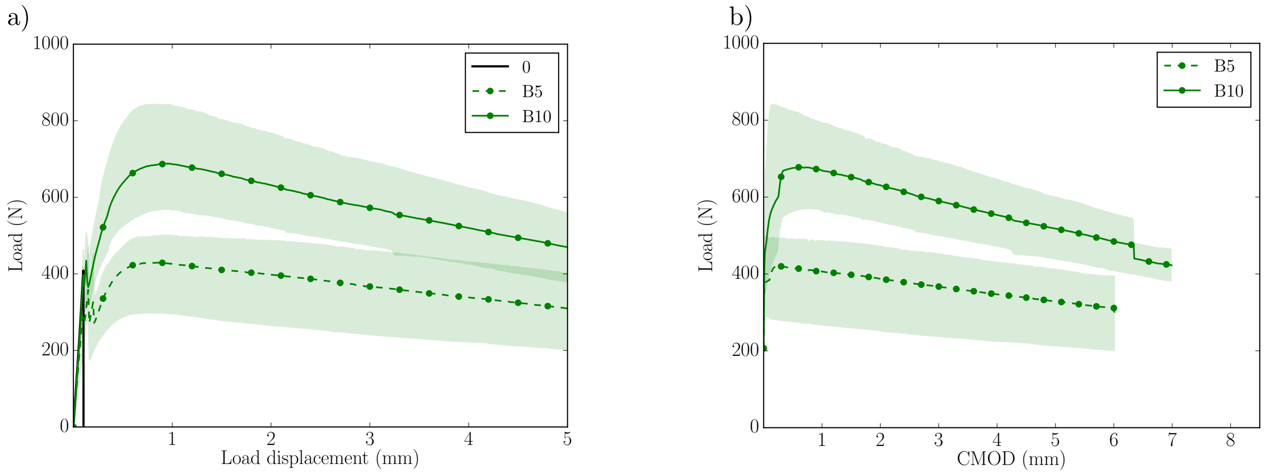

Figure 6: Experimental results of the three-point bending tests on specimens manufactured with B fibres (shaded areas represent the experimental envelopes).

Table 2: Specific fracture energy in N/m at different load displacements and ratio with respect to mix 0.

Mix	Load displacement					
	1 mm		3 mm		5 mm	
	G_F (N/m)	$\frac{G_{Fi}}{G_{F0}}$	G_F (N/m)	$\frac{G_{Fi}}{G_{F0}}$	G_F (N/m)	$\frac{G_{Fi}}{G_{F0}}$
0	23.97	1.00	23.97	1.00	23.97	1.00
A5	77.93	3.25	229.61	9.58	347.01	14.48
A10	164.37	6.86	501.94	20.94	751.86	31.36
B5	337.34	14.07	1072.95	44.76	1699.65	70.90
B10	519.72	21.68	1687.27	70.38	2649.93	110.54
C5-L24	96.09	4.01	181.29	7.56	229.00	9.55
C10-L24	354.71	14.80	1261.63	52.63	1992.61	83.12
C5-L48	392.96	16.39	1448.90	60.44	2322.01	96.86
C10-L48	112.06	4.67	217.73	9.08	263.04	10.97
C5-L60	531.69	22.18	1733.76	72.32	2408.07	100.45
C10-L60	561.69	23.43	2070.04	86.35	3249.15	135.54

$\delta = 5$ mm, which is expected to grow higher at larger values of δ.

Finally, in order to analyse how each type of fibre induced different fracture mechanisms, the value of the CMOD and the load displacement have been compared at an advanced state of the test, specifically at $\delta = 5$ mm. These results can be consulted in Table 3 and are displayed in Figure 9. It can be observed that the use of A type microfibres lead to higher values of the CMOD/δ ratio, especially if the values obtained with 24 long C type fibres are ignored since, as explained before, they are not representative of the possibilities of these fibres as reinforcement of gypsum. A type specimens provide ratios of around 1.4-1.6 while the other specimens give values of 0.9-1.3. This means that the use of A type microfibres tends to produce more visible cracks than the use of B or C types macrofibres. This can be more clearly understood with the help of the DIC results. Figure 10 shows the horizontal strain fields of three specimens obtained with the DIC analysis, which correspond to A5, B5 and C5-L48 specimens. All the three images show the horizontal strain field at the same load displacement ($\delta = 5$ mm), which allows comparing the three types of fibres considered in this study. In the case of the A5 and B5 specimens, damage develops in a very concentrated crack path, following an almost straight line connecting the initial crack tip and the load application point, while in the case of the C5-L48 specimen, the strain field allows identifying several cracks that extend along a certain width of the specimen. Therefore, A type microfibres induce a fracture mechanism that concentrates damage in a single crack while C type macrofibres extend the damage mechanism to a wider region of the specimen, inducing

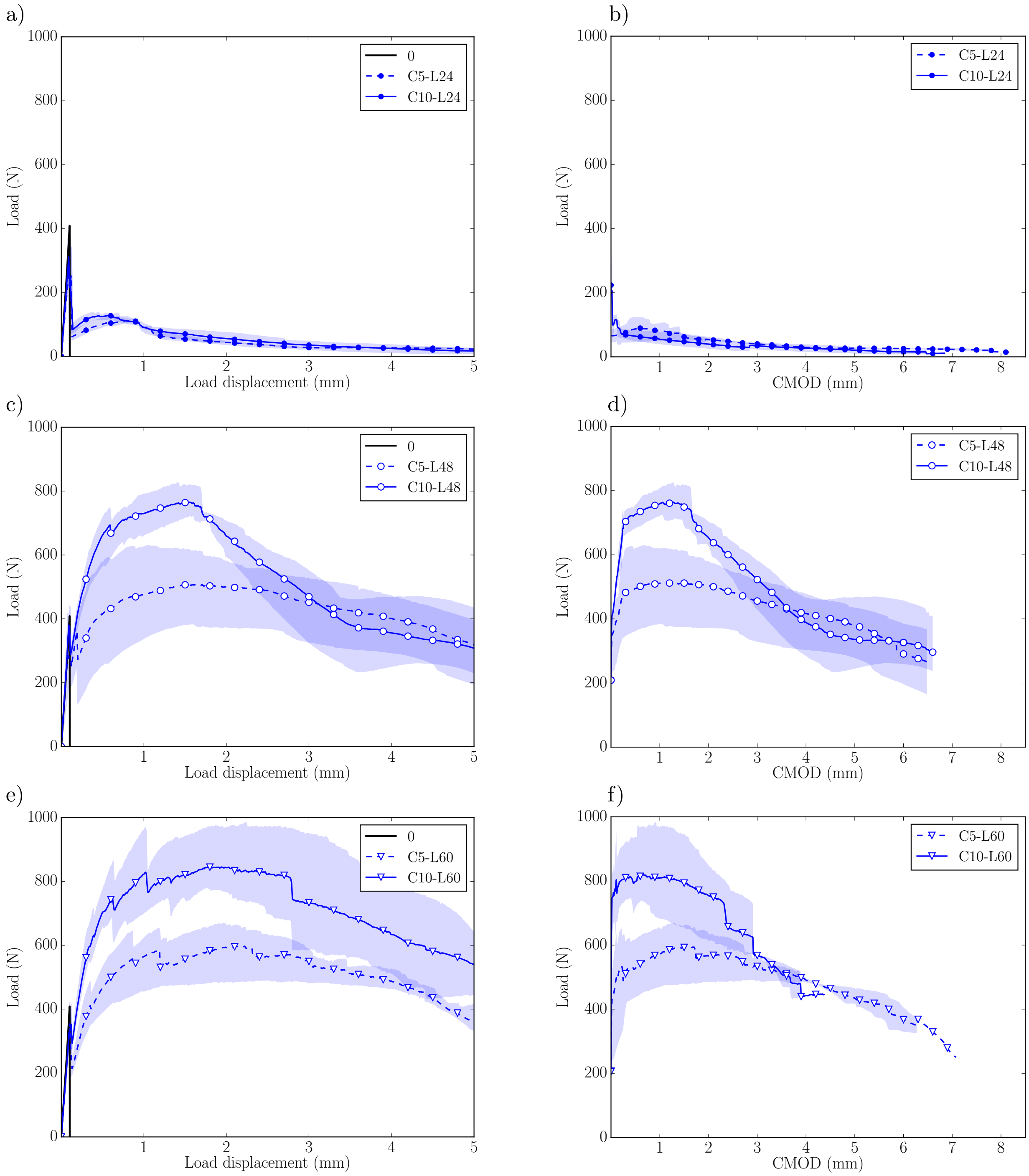

Figure 7: Experimental results of the three-point bending tests on specimens manufactured with C fibres (shaded areas represent the experimental envelopes).

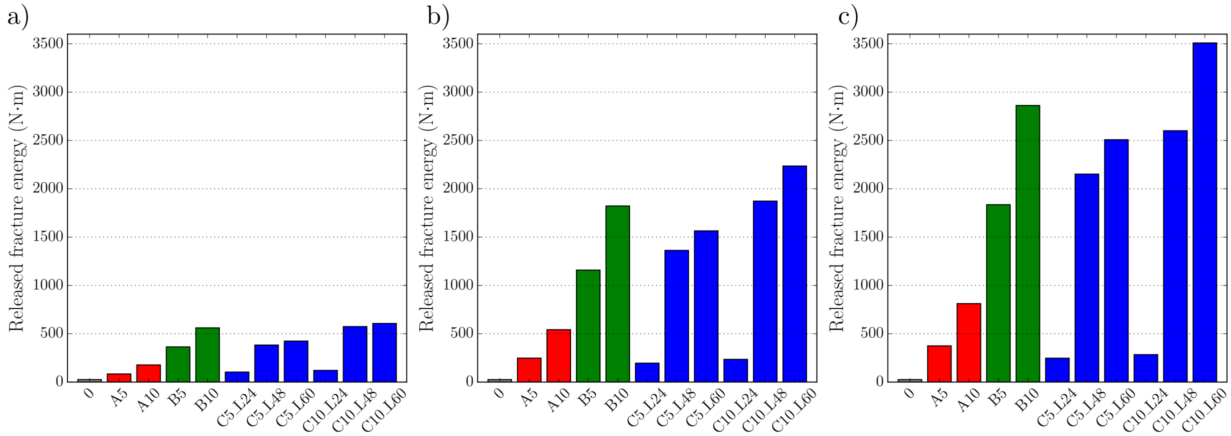

Figure 8: Released energy of each mix at three instants of the test: a) $\delta = 1$ mm, b) $\delta = 3$ mm and c) $\delta = 5$ mm.

Table 3: Comparison of CMOD versus load displacement at $\delta = 5$ mm.

Mix	Load displacement (mm)	CMOD (mm)	CMOD/δ
A5	5.0	8.15	1.63
A10	5.0	7.15	1.43
B5	5.0	5.90	1.18
B10	5.0	6.35	1.27
C5-L24	5.0	7.37	1.47
C10-L24	5.0	5.62	1.12
C5-L48	5.0	5.86	1.17
C10-L48	5.0	6.46	1.29
C5-L60	5.0	6.10	1.22
C10-L60	5.0	4.63	0.93

several small cracks that, as a result, produce a thinner main crack. This results in different values of the crack tip opening displacement, which as the figure clearly shows, is much smaller in the case of C5-L48 specimen when compared with any of the other two specimens.

4.3. Compression test

Figure 11 shows the results obtained with the compression tests for each FRG mix compared with plain gypsum. The values of σ_{max} have been obtained as F_{max}/S with F_{max} being the maximum compression load and S the compression surface (40×40 mm^2).

Figures 11c and 11d show that the specimens made with B type fibres and 48 and 60 mm long C type fibres show no significant differences with respect to plain gypsum specimens, only a slight trend to lower values of the maximum compression strength can be highlighted.

The load-displacement diagrams show that the specimens made with A type microfibres tend to have a lower modulus of elasticity and a lower maximum compressive strength, which can also be observed in Figures 11a and 11b, where A5 and A10 show lower peak loads and elastic slopes. This suggests that the microfibres modify the overall elastic mechanical properties of gypsum, giving rise to some extent to a new material with different characteristics. In the case of specimens made of B and C type fibres, these differences are not so evident and it seems that the elastic behaviour of the material is similar to that of plain gypsum.

Figures 11a and 11b also show interesting differences among these mixes. With regard to A type specimens, although the peak load is lower, the load decay after it is smoother, only experiencing a small decrease as the test proceeds. In the case of C type specimens, the pre-peak behaviour is very similar, but after the peak, they show a faster load decrease than A type specimens, while B type specimens show an intermediate load decrease, not as fast as C type ones neither as slow as A type specimens. This suggest that in the case of the

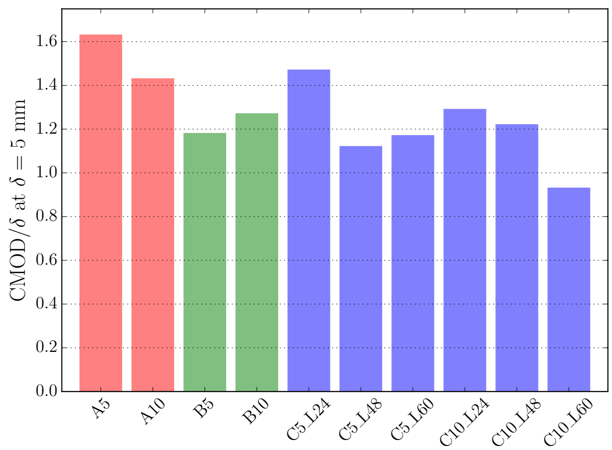

Figure 9: Comparison of the CMOD/δ ratio when $\delta = 5$ mm.

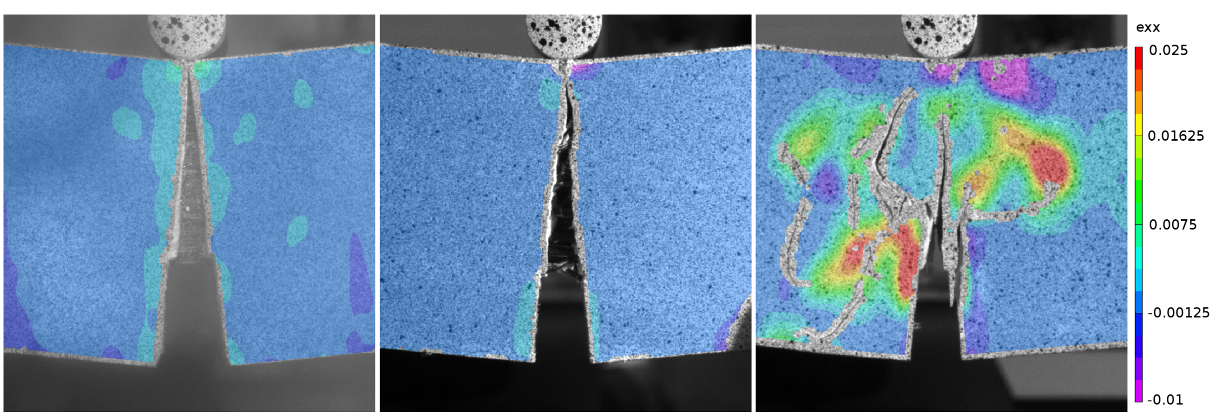

Figure 10: Comparison of ε_x strain fields of A5 (left), B5 (center) and C5-L48 (right) specimens at a load displacement of $\delta = 5$ mm.

Table 4: Values of E and σ_{max} in the compression tests and the corresponding ratios with respect to mix 0; coefficients of variation (or relative standard deviations) are reported in brackets.

Mix	E (MPa)	$\frac{E_i}{E_0}$	σ_{max} (MPa)	$\frac{\sigma_{max_i}}{\sigma_{max_0}}$
0	922.26 (0.03)	1.00	11.94 (0.04)	1.00
A5	797.44 (0.01)	0.86	10.77 (0.11)	0.90
A10	860.59 (0.10)	0.93	9.47 (0.04)	0.79
B5	938.68 (0.06)	1.02	11.73 (0.05)	0.98
B10	897.48 (0.05)	0.97	11.31 (0.10)	0.95
C5-L24	927.86 (0.07)	1.01	12.70 (0.06)	1.06
C5-L48	919.99 (0.08)	1.00	12.16 (0.07)	1.02
C5-L60	959.26 (0.05)	1.04	11.15 (0.05)	0.93
C10-L24	959.34 (0.03)	1.04	11.96 (0.09)	1.00
C10-L48	926.68 (0.03)	1.00	10.63 (0.06)	0.89
C10-L60	924.49 (0.04)	1.00	11.22 (0.07)	0.94

specimens manufactured with type A microfibres, there is a certain confinement of the material, probably due to the effect of the fibres embracing the tensile stresses indirectly induced by compression and containing to some extent the tensile cracking.

Finally, Figure 12 shows the aspect of three representative specimens of each type of fibre at the end of the compression test compared with a mix without fibres. It is worth observing that A type microfibres tend to distribute damage at the whole specimen, producing a very scattered cracking pattern and not producing almost any dust or loose scrap around it. On the contrary, C type specimens tend to concentrate damage along the fibres, inducing spalling and a considerable amount of dust and loose scraps of gypsum around the specimen, although not as much as plain gypsum. As regards B type specimens, although damage tends to be more concentrated than in the case of A type ones, the dust or loose scraps around the specimens are almost non-existent. It is interesting to observe how both, A and B type fibres, show a certain containing effect regarding the material cracking and splitting, but the A type fibres also induce certain confinement in the material that helps to extend the maximum compression strength for larger displacement values, which cannot be observed in specimens made with B type fibres.

4.4. Pull-out test

The pull-out tests have only been carried out with C type fibres, since the micro nature of A type fibres make them difficult to analyse with this test and the B fibres are considered not to provide easily comparable results, given that the ramifications at their endings modify the resistant mechanism which no longer depends only on the fibre-gypsum bonding interface.

Figure 13 displays the load-slip diagrams obtained for three fibre-embedding lengths: 10, 20 and 30 mm. The blue shades represent the experimental envelope for each length and the lines the average diagrams.

In all three cases, the load increases up to a first maximum, then decreases down to a local minimum and continues with increasing-decreasing cycles where the local maximum becomes smaller as the test progresses. The cadence of the local maxima is in all three cases around 2 mm, which suggests that these load oscillations are directly related to the shape pattern of C-type fibres, which is repeated every 2 mm, as can be observed in Figure 1.

The first maximum load increases with the embedding length, as expected, presenting values of around 210, 160 and 110 N for embedding lengths of 30, 20 and 10 mm, respectively. It is interesting and somewhat surprising to see that the first maximum load is for all three embedding lengths similar to those obtained in [34] for cement mortar, a significantly stronger matrix ($\approx$ 225 N for L = 30 mm, $\approx$ 160 N for L = 20 mm and $\approx$ 130 N for L = 10 mm). This suggests that the bonding mechanism of this type of fibres relies mainly on the fibre and not clearly on the strength of the matrix. The explanation for the progressive decay of the local maximum loads is pretty straightforward, since as the fibre is pulled out of the gypsum matrix, a shorter length of fibre remains inside, thus the bonding mechanism becomes weaker. Nevertheless, the first load decay is always significantly higher that the rest in all cases, which could be due to the fact that the

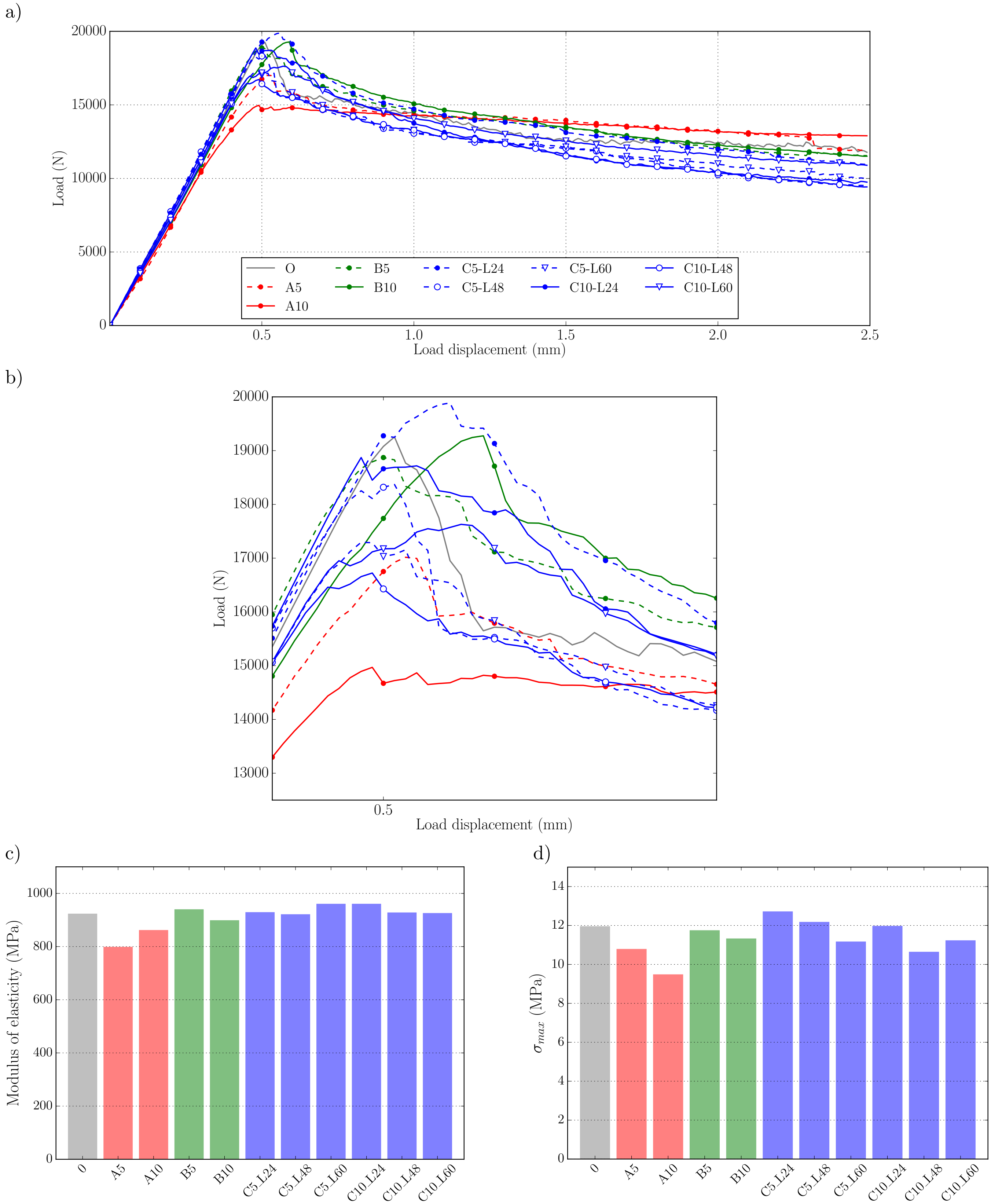

Figure 11: Experimental results of the compression tests: a) load-displacement diagrams, b) detail of the peaks in the load-displacement diagrams, c) average modulus of elasticity and d) average maximum compression stress.

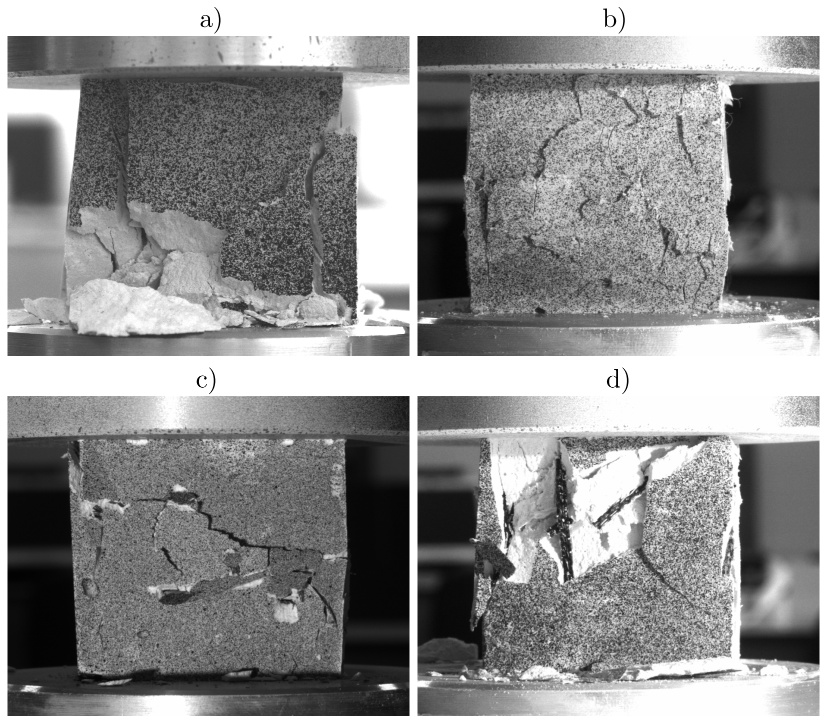

Figure 12: Images of specimens after the compression test is finished: a) 0 type specimen, b) A type specimen, c) B type specimen and d) C type specimen (L=48 mm).

matrix in contact with the fibre is intact at the beginning of the test, but after the first decay, it is slightly polished by the fibre displacement, thus offering smaller resistance to the pulling out of the fibre.

The failure always results from fibre-matrix debonding and slipping, but not from the breakage of the fibre. This is in agreement with the experimental results, where no broken fibre was found, but fibres were always pulled out from gypsum. Longer embedding lengths could lead to different results, but since the maximum fibre length is in this study equal to 60 mm in an ideal case, the maximum embedding length would be 30 mm, which coincides with the maximum length considered in the pull-out test. These results are in accordance with the three-point bending analyses. Given that fibres embedded 30 mm were still pulled-out and did not reach the maximum tensile strength of the fibres, the critical length of this fibre type in gypsum is higher than 30mm. This explains the better results for 60 mm long fibres.

It is worth noting that only the case of fibres oriented parallel to the load direction is considered. The orientation of the fibres with respect to the load direction has a strong influence on this problem, as studied in [34], therefore these results are only a first approximation to the problem and they can be complemented in future research.

5. Conclusions

In this paper the mechanical and fracture behaviour of polymer-fibre reinforced specimens was studied, using micro and macrofibres with different surface finishings and lengths. The main conclusions can be summarised as follows:

- The fibre size has a strong influence on the fresh state of the mix, leading to less workable mixes when microscopic fibres are used. The micro size of the fibres lead to higher amount of water attached to them, thus producing a thicker mix.

- In general, both macrofibres used in this study (B and C) have a better performance in fracture if compared with the microfibres A.

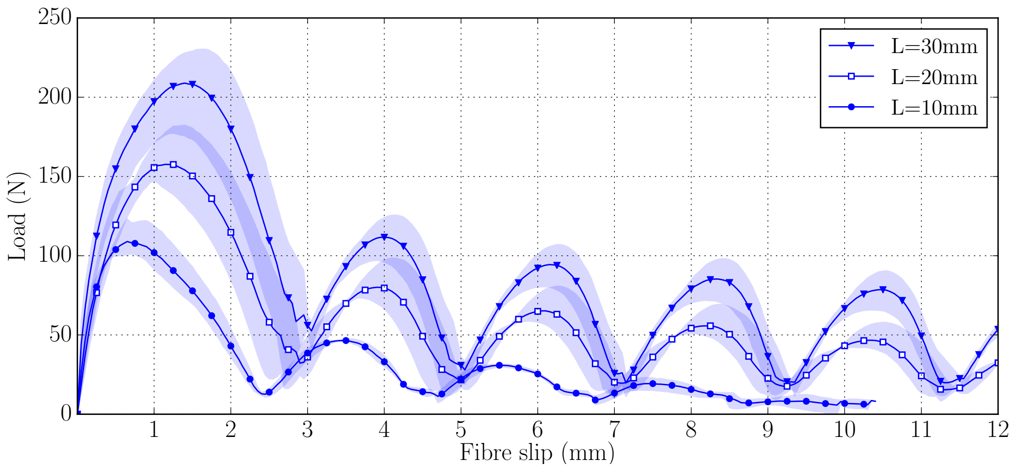

Figure 13: Experimental results of the pull-out tests on specimens manufactured with C fibres

- In the case of the macrofibres, the fibre length is of paramount importance. Since the gypsum matrix is relatively weak, in the case of macrofibres, failure is always the result of the debonding of the fibres and the matrix, therefore, longer fibres provide better performance. When too short fibres are used (L=24mm) the efficiency of the reinforcement is surprisingly low.

- The surface finishing of the macrofibres modifies their fracture behaviour. In the case of the embossed surface fibres (C type), the load displacement diagrams of the three-point bending tests present abrupt load changes related to this issue, while in the case of B type fibres, the diagrams are smooth. The macro nature of B and C fibres tends to concentrate the fibre reinforcement in very specific zones of the specimen, thus greatly improving the mechanical properties in some regions and not affecting others, whereas the micro nature of A fibres strengthen the gypsum matrix in a uniform way.

- The use of embossed surface macrofibres (type C) leads to a distribution of the fracture processes over a wider region in the gypsum matrix, thus smaller values of crack opening, especially in the case of longer fibres (L=60 mm). This type of surface finishing improves the fibre anchorage with the gypsum matrix and makes it more efficient, thus extending their reinforcement to higher values of the load displacement.

- The use of fibres greatly increase the released energy of the material during the fracture process, being remarkably high in the case of relatively long macrofibres (B and C with lengths of 48 and 60 mm).

- Under compression, the use of microfibres slightly reduce the elastic-modulus of the material and the maximum bearing load, which is not observed in the case of specimens manufactured with macrofibres. Microfibres uniformly modify the microstructure of the material at a microscopic scale and can be seen as a new material itself before damage begins. In the case of specimens reinforced with macrofibres, the material behaviour before damage begins is similar to unreinforced gypsum because, at a microscopic scale, the load is born by gypsum itself; fibres only begin to modify the material behaviour when damage begins.

- The use of microfibres seems to induce a certain confinement effect which reduce the load decay after peak in the compression tests.

- Further studies about the fibre orientation factor for the manufacture processes used in FRG could improve the reliability of this material for future applications.

- The results of this study have shown that there is a wide range of possible applications of gypsum reinforced with polymer fibres.

Acknowledgements

The authors gratefully acknowledge the financial support provided by the Ministry of Economy and Competitiveness of Spain through the Research Fund Project BIA2016-78742-C2-2-R. They also wish to thank Sika for providing the fibres used in this study and wish to thank Gabriel Pardo for their valuable comments at the first stages of the experimental work.

References

[1] Zollo RF. Fiber-reinforced concrete: an overview after 30 years of development. Cement and Concrete Composites. 1997;19(2):107 – 122. Available from: http://www.sciencedirect.com/science/article/pii/S0958946596000467.

[2] Banthia N, Gupta R. Influence of polypropylene fiber geometry on plastic shrinkage cracking in concrete. Cement and Concrete Research. 2006;36(7):1263 – 1267. Available from: http://www.sciencedirect.com/science/article/pii/S0008884606000056.

[3] Bentur A, Mindess S. Fibre reinforced cementitious composites. CRC Press; 2014.

[4] Alberti MG, Enfedaque A, Gálvez JC. Comparison between polyolefin fibre reinforced vibrated conventional concrete and self-compacting concrete. Construction and Building Materials. 2015;85:182 – 194. Available from: http://www.sciencedirect.com/science/article/pii/S0950061815002548.

[5] Beverly P. fib model code for concrete structures 2010. Ernst & Sohn; 2013.

[6] DBV, Merkblatt StahlfaserbetonDeutsche Beton Vereins, Guide to Good Practice. German Society for Concrete and Construction Technology; 2001.

[7] CNR-DT 204/2006. Guide for the design and construction of fiber-reinforced concrete structures. Consiglio Nazionale delle Riserche, Rome, Italy; 2006.

[8] EHE-08, Spanish Structural Concrete Code. Spanish Minister of Public Works, Madrid, Spain; 2008.

[9] Alberti MG, Enfedaque A, Gálvez JC, Agrawal V. Reliability of polyolefin fibre reinforced concrete beyond laboratory sizes and construction procedures. Composite Structures. 2016;140:506 – 524. Available from: http://www.sciencedirect.com/science/article/pii/S0263822315011587.

[10] García Santos A. Comportamiento mecánico de yeso reforzado con polímeros sintéticos. Universidad Politécnica de Madrid; 1988.

[11] Santos AG. PPF-reinforced, ESP-lightened gypsum plaster. Materiales de construcción. 2009;59(293):105–124.

[12] del Mar Barbero-Barrera M, Flores-Medina N, Pérez-Villar V. Assessment of thermal performance of gypsum-based composites with revalorized graphite filler. Construction and Building Materials. 2017;142:83–91.

[13] Zhu C, Zhang J, Peng J, Cao W, Liu J. Physical and mechanical properties of gypsum-based composites reinforced with PVA and PP fibers. Construction and Building Materials. 2018;163:695–705.

[14] Medina NF, Barbero-Barrera MM. Mechanical and physical enhancement of gypsum composites through a synergic work of polypropylene fiber and recycled isostatic graphite filler. Construction and Building Materials. 2017;131:165–177.

[15] Dalmay, Pierre and Smith, Agnès and Chotard, Thierry and Sahay-Turner, P and Gloaguen, Vincent and Krausz, Pierre. Properties of cellulosic fibre reinforced plaster: influence of hemp or flax fibres on the properties of set gypsum. Journal of materials science. 2010;45(3):793–803.

[16] Fabio Iucolano and Barbara Liguori and Paolo Aprea and Domenico Caputo. Evaluation of bio-degummed hemp fibers as reinforcement in gypsum plaster. Composites Part B: Engineering. 2018;138:149 – 156. Available from: http://www.sciencedirect.com/science/article/pii/S1359836817322023.

[17] Fabio Iucolano and Luca Boccarusso and Antonio Langella. Hemp as eco-friendly substitute of glass fibres for gypsum reinforcement: Impact and flexural behaviour. Composites Part B: Engineering. 2019;175:107073. Available from: http://www.sciencedirect.com/science/article/pii/S135983681931337X.

[18] Behfarnia K, Behravan A. Application of high performance polypropylene fibers in concrete lining of water tunnels. Materials & Design. 2014;55:274–279.

[19] Alberti MG, Enfedaque A, Gálvez JC, Pinillos L. Structural Cast-in-Place Application of Polyolefin Fiber–Reinforced Concrete in a Water Pipeline Supporting Elements. Journal of Pipeline Systems Engineering and Practice. 2017;8(4):05017002.

[20] Enfedaque A, Alberti M, Gálvez J, Rivera M, Simón-Talero J. Can Polyolefin Fibre Reinforced Concrete Improve the Sustainability of a Flyover Bridge? Sustainability. 2018;10(12):4583.

[21] Alberti MG, Gálvez JC, Enfedaque A, Carmona A, Valverde C, Pardo G. Use of Steel and Polyolefin Fibres in the La Canda Tunnels: Applying MIVES for Assessing Sustainability Evaluation. Sustainability. 2018;10(12):4765.

[22] Medina NF, Barbero-Barrera MM. Mechanical and physical enhancement of gypsum composites through a synergic work of polypropylene fiber and recycled isostatic graphite filler. Construction and Building Materials. 2017;131:165 – 177. Available from: http://www.sciencedirect.com/science/article/pii/S0950061816318335.

[23] Zhu C, Zhang J, Peng J, Cao W, Liu J. Physical and mechanical properties of gypsum-based composites reinforced with PVA and PP fibers. Construction and Building Materials. 2018;163:695 – 705. Available from: http://www.sciencedirect.com/science/article/pii/S0950061817325734.

[24] Enfedaque A, Gálvez JC, Suárez F. Analysis of fracture tests of glass fibre reinforced cement (GRC) using digital image correlation. Construction and Building Materials. 2015;75:472 – 487. Available from: http://www.sciencedirect.com/science/article/pii/S0950061814012434.

[25] Lakavath C, Joshi SS, Prakash SS. Investigation of the effect of steel fibers on the shear crack-opening and crack-slip behavior of prestressed concrete beams using digital image correlation. Engineering Structures. 2019;193:28 – 42. Available from: http://www.sciencedirect.com/science/article/pii/S0141029618335880.

[26] UNE-EN 13279-2: Gypsum binders and gypsum plasters - Part 2: Test methods; 2014.

[27] UNE-EN 13279-1: Gypsum binders and gypsum plasters - Part 1: Definitions and requirements; 2009.

[28] Chu T, Ranson W, Sutton MA. Applications of digital-image-correlation techniques to experimental mechanics. Experimental mechanics. 1985;25(3):232–244.

[29] Sutton MA, Orteu JJ, Schreier H. Image correlation for shape, motion and deformation measurements: basic concepts, theory and applications. Springer Science & Business Media; 2009.

[30] Solutions C. Vic-2D. Reference Manual. 2009;.

[31] Schindelin J, Rueden CT, Hiner MC, Eliceiri KW. The ImageJ ecosystem: An open platform for biomedical image analysis. Molecular reproduction and development. 2015;82(7-8):518–529.

[32] Enfedaque A, Alberti MG, Gálvez JC. Influence of Fiber Distribution and Orientation in the Fracture Behavior of Polyolefin Fiber-Reinforced Concrete. Materials. 2019;12(2):220.

[33] Suárez F, Gálvez J, Enfedaque A, Alberti M. Modelling fracture on polyolefin fibre reinforced concrete specimens subjected to mixed-mode loading. Engineering Fracture Mechanics. 2019;211:244–253.

[34] Alberti M, Enfedaque A, Gálvez J, Ferreras A. Pull-out behaviour and interface critical parameters of polyolefin fibres embedded in mortar and self-compacting concrete matrixes. Construction and Building Materials. 2016;112:607–622.